Kunisaki Shaun (Orcid ID: 0000-0002-9229-4733)

Human induced pluripotent stem cell-derived lung organoids in an *ex vivo* model of the congenital diaphragmatic hernia fetal lung

Shaun M. Kunisaki, MD, MSc[1,2]; Guihua Jiang, MS[3]; Juan C. Biancotti, PhD[1,2]; Kenneth K.Y. Ho, PhD[4]; Briana R. Dye, PhD[5]; Allen P. Liu, PhD[4]; and Jason R. Spence, PhD[5,6]

[1]Department of Surgery, Johns Hopkins University, Baltimore, MD 21287, USA
[2]Institute for Cell Engineering, Johns Hopkins University, Baltimore, MD 21287, USA
[3]Department of Surgery, University of Michigan, Ann Arbor, MI 48109, USA
[4]Department of Mechanical Engineering, University of Michigan, Ann Arbor, MI 48109, USA
[5]Department of Cell and Developmental Biology, University of Michigan, Ann Arbor, MI 48109, USA
[6]Department of Internal Medicine, University of Michigan, Ann Arbor, MI 48109, USA

Running Title: Human iPSC lung organoids in diaphragmatic hernia

Author Contributions
Shaun Kunisaki: Conception and design, financial support, provision of study material/patients, data analysis and interpretation, manuscript writing
Guihua Jiang: Conception and design, collection and assembly of data, data analysis and interpretation, manuscript writing, final approval of manuscript
Juan Biancotti: Collection and assembly of data, data analysis and interpretation, manuscript writing, final approval of manuscript
Kenneth Ho: Collection and assembly of data, data analysis and interpretation, final approval of manuscript
Briana Dye: Collection and assembly of data, data analysis and interpretation, final approval of manuscript
Allen Liu: Conception and design, data analysis and interpretation, final approval of manuscript
Jason Spence: Conception and design, financial support, data analysis and interpretation, final approval of manuscript

Corresponding Author:
Shaun M. Kunisaki, MD, MSc
Associate Professor of Surgery
Johns Hopkins University School of Medicine
1800 Orleans Street, Suite 7353

This is the author manuscript accepted for publication and has undergone full peer review but has not been through the copyediting, typesetting, pagination and proofreading process, which may lead to differences between this version and the Version of Record. Please cite this article as doi: 10.1002/sctm.12826

Baltimore, MD 21287 USA
Email: skunisa1@jhmi.edu
Phone: (410) 955-6256, Fax: (410) 502-5314

Keywords: congenital diaphragmatic hernia, fetal lung, mechanical compression, lung organoids, induced pluripotent stem cells

Abstract

Three-dimensional lung organoids derived from pluripotent stem cells have the potential to enhance our understanding of disease mechanisms and to enable novel therapeutic approaches in neonates with pulmonary disorders. We established a reproducible *ex vivo* model of lung development using transgene-free human induced pluripotent stem cells generated from fetuses and infants with Bochdalek congenital diaphragmatic hernia (CDH), a polygenic disorder associated with fetal lung compression and pulmonary hypoplasia at birth. Molecular and cellular comparisons of CDH lung organoids revealed impaired generation of $NKX2.1^{+}$ progenitors, type II alveolar epithelial cells, and $PDGFR\alpha^{+}$ myofibroblasts. We then subjected these lung organoids to disease relevant mechanical cues through *ex vivo* compression and observed significant changes in genes associated with pulmonary progenitors, alveolar epithelial cells, and mesenchymal fibroblasts. Collectively, these data suggest both primary cell-intrinsic and secondary mechanical causes of CDH lung hypoplasia and support the use of this stem cell-based approach for disease modeling in CDH.

Graphical Abstract: We established a reproducible *ex vivo* model of lung development using transgene-free human induced pluripotent stem cells generated from fetuses and infants with Bochdalek congenital diaphragmatic hernia. Both primary cell-intrinsic and secondary causes of CDH lung hypoplasia were identified, and mechanical compression was associated with alterations in lung organoid epithelial and mesenchymal gene regulation.

Keywords: congenital diaphragmatic hernia, fetal lung, mechanical compression, lung organoids, induced pluripotent stem cells

1. Introduction

Bochdalek congenital diaphragmatic hernia (CDH), a condition associated with pulmonary hypoplasia at birth, is one of the most common, costly, and severe birth defects managed by neonatologists and pediatric surgeons worldwide.[1,2] The overall mortality rate in neonates born with CDH is 30%, and there is a wide spectrum of morbidity based largely on the degree of pulmonary disease.[3] In those born with the severe disease phenotype, state-of-the-art advances in critical care, including novel pharmacologic targets, non-conventional ventilator strategies, extracorporeal membrane oxygenation, and fetal tracheal occlusion surgery, have failed to make a substantial impact in terms of improving outcomes.[4-6] Moreover, among survivors with CDH, there are often chronic, long-term problems that persist for years, as validated by the spawning of multidisciplinary clinics dedicated to the care of these patients at major children's hospitals.[7,8] A better understanding of disease pathogenesis of the CDH lung is needed if further inroads are to be made in the management of this debilitating condition.

The underlying cause of CDH remains unknown.[9] Although family cohorts with an autosomal dominant inheritance have been reported, the vast majority of cases are sporadic,[10] and no single genetic mutation accounts for more than 1-2% of cases.[11,12] Through molecular cytogenetic analyses, studies have identified copy number variants and chromosomal regions through which over 50 candidate CDH-causative genes have

been proposed in humans.[13-15] Functional analyses of these genes using animal models have been difficult due to early embryonic lethality, lack of conditional mutants, and low/variable recapitulation of the CDH phenotype.[15,16]

Physical environmental factors have increasingly been shown to regulate lung organogenesis.[17] In the case of CDH, there has been a long-standing belief that the associated lung abnormalities are primarily caused by mechanical compression of the developing lung upon failed closure of one of the pleuroperitoneal canals at eight weeks gestation.[18] The abdominal contents, usually liver and intestines, subsequently herniate through the diaphragmatic defect *in utero*, causing mass effect during the pseudoglandular and canalicular stages of pulmonary development. Evidence in support of a mechanical mechanism has been shown experimentally through surgical creation of a diaphragmatic defect in fetal lambs, which universally induces lung hypoplasia at term.[19] Clinical studies of children with CDH have also shown that the volume of abdominal herniation in the fetus significantly correlates with the severity of lung hypoplasia and clinical disease.[20]

The classical paradigm of mechanical compression-induced lung hypoplasia has been challenged by a number of investigators based on several important observations.[21-24] First, despite the fact that the diaphragmatic defect is almost always limited to only one of the hemi-diaphragms, the observed pulmonary hypoplasia and pulmonary hypertension also affects the contralateral lung, albeit to a lesser degree.[9]

Second, other space-occupying lesions where there is extrinsic mass effect on early fetal lung development (e.g., congenital lung malformations) are not typically associated with significant lung hypoplasia and pulmonary hypertension at birth.[24] Third, teratogenic rodent models of CDH (e.g., nitrofen, bisdiamine) have suggested that abnormal lung morphogenesis starts as early as E11, either in the absence of any diaphragmatic defect or before the diaphragm has completely formed at E16.[25,26] Taken together, these observations suggest that there may be primary cell-based defects in CDH lung morphogenesis that are merely exacerbated by exposure to mechanical compression forces.[27]

Given these fundamental questions regarding the embryologic origins of CDH pulmonary hypoplasia, we sought to develop a human stem cell-based strategy for modeling fetal lung development and for determining the future potential for cell-based treatment strategies in CDH. Our approach involved the directed differentiation of human induced pluripotent stem cells (iPSCs) from CDH patients into three-dimensional (3D) lung organoids (LOs) containing both pulmonary epithelial and mesenchymal cell types. Based on results from CDH LOs generated from clones derived from six affected patients, these LOs possessed airway-like epithelial structures, alveolar cell types, and mesenchyme most closely corresponding to the pseudoglandular and early canalicular stages of lung development. In the absence of mechanical forces, comparisons of CDH lung organoids with those derived from normal (non-CDH) controls revealed impaired

expression of NKX2.1^{+} lung progenitors, type II alveolar epithelial cells, and platelet derived growth factor receptor-alpha^{+} (PDGFRα) myofibroblasts.

To recapitulate the lung compression that occurs *in utero*, we then applied mechanical forces to CDH organoids during the pseudoglandular stage of differentiation. We observed significant downregulation of *NKX2.1* as well as *SOX2* and *SOX9*, genes associated with proximal and distal lung progenitor differentiation, respectively. Mechanical compression also correlated with significant upregulation of pro-fibrotic mesenchymal fibroblast genes. Collectively, these data support the notion of both primary cell-intrinsic and secondary mechanical causes in the maldevelopment of the CDH lung. Further study of this research platform will be instrumental for elucidating the disease-relevant mechanical cues and critical epithelial-mesenchymal interactions that contribute to early lung development in CDH.

2. Materials and Methods

2.1. Human Tissue

De-identified human amniotic fluid and neonatal foreskin samples were obtained by consent under approved institutional review board protocols at the Johns Hopkins University (IRB #202082) and the University of Michigan (IRB #38565). Amniotic fluid samples (8-10 mL) were obtained by amniocentesis from confirmed cases of CDH by prenatal ultrasound (n=2) as well as from normal fetuses without CDH (n=2) at 18-24

weeks gestation (Table S1).[28] Foreskin specimens were also obtained from male CDH (n=4) and normal (n=2) infants following elective circumcision. Isolation of somatic cells was performed as previously described in our laboratory.[28,29]

As controls, blocks of human normal and CDH lung tissue (n=4) from fetuses/neonates were obtained under the same institutional review board approval at the University of Michigan.

2.2. iPSC Derivation

All work was carried out under oversight committee approval (HPSCRO #1044). iPSCs were generated using non-integrating, cytoplasmic Sendai Virus (CytoTune™-iPS Reprogramming Kit, Invitrogen, Waltham, MA) as previously described.[28,29] Embryoid bodies (EB) were formed in suspension culture and analyzed using standard methods.[30] Karyotyping was performed on iPSCs by Cell Line Genetics (Madison, WI). Individual staining and measurements were performed in triplicate.

2.3. Lung Organoid Generation

Differentiation of iPSCs into definitive endoderm and subsequently into ventral-anterior foregut spheroids was carried out using a protocol as detailed elsewhere.[31,32] Briefly, iPSCs were treated with 100 ng/mL Activin A (R&D Systems, Minneapolis, MN) and then incubated in foregut media: DMEM/F12 (Invitrogen) containing N2 and B27

(Thermo Fisher, Waltham, MA), 10 mM HEPES (Thermo Fisher), 200 ng/mL Noggin (R&D), 10µM SB431542 (Stemgent, Cambridge, MA), 2µM Chiron (Stemgent), 500 ng/mL FGF4 (R&D), and 1µM SAG (Enzo Life Science, Farmingdale, NY) for 8 days. Cells (25 organoids/well) were resuspended in 50 µL Matrigel (BD, Franklin Lakes, NJ), and LOs were maintained in a 24-well plate with 500 ng/mL FGF10 (R&D) until the study endpoint of 20, 40, or 60 days.

2.4. Compression Testing

The compression device was based on work described elsewhere[33] with some modifications (Figure 6A) and has been previously reported.[34] Briefly, day-40 CDH LOs (n=10 per drop) were encapsulated into 50 µl of Matrigel and placed onto 0.4 µm pore size PET transwell membranes (Fisher Scientific, 07-200-170, Waltham, MA). CDH and normal LOs were overlaid with a 1% agarose gel cushion (Invitrogen, Ultra-Pure Agarose, 16500-100) made from sterilized 24-mm PDMS molds. A weighted object corresponding to a predetermined compression force (range, 0-400 Pa) was applied for 48 hrs prior to further analyses. Forces were chosen based on *in vitro* and *in vivo* work described elsewhere.[17,35]

2.5. Histology and Immunofluorescence

All samples were fixed in paraformaldehyde. Confirmation of alkaline phosphatase (AP) expression within iPSCs was performed using the AP substrate kit (Millipore, Burlington, MA) according to the manufacturer's instructions. Organoids and tissues were embedded in paraffin and sectioned at 5 μm prior to staining. In preparation for immunofluorescence, sections underwent antigen retrieval with pH 9.0 Tris/EDTA Buffer. Human CDH lung tissue blocks (n=6) were obtained for comparative analysis from the University of Michigan Department of Pathology (courtesy of Dr. Raja Rabah). Staining was carried out as previously described.[31] The antibodies and dilutions used are shown in Table S4. Slides were imaged using a Nikon A1 confocal microscope (Melville, NY) or an Olympus IX71 epifluorescent microscope (Center Valley, PA). Cell quantification based on confocal images was performed in a blinded fashion from at least five sections per LO using ImageJ with a cell counter plugin.[31] The total number of cells was determined by $DAPI^+$ nuclei with the same section.

2.6. RNA Extraction and qPCR

RNA was extracted using the MagMAX-96 Total RNA Isolation Kit (Life Technologies, Carlsbad, CA) and MAG Max Express (Applied Biosystems, Grand Island, NY). RNA concentration was measured with NanoDrop 2000 (Thermo Fisher). Reverse transcription was conducted using the SuperScript VILO kit (Invitrogen) and quantitative RT-PCR was carried out using Fast SYBR Green Master Mix (Applied

Biosystems) on an AB-QuantStudio3 real time PCR machine (Thermo Fisher). The primer sequences can be found in Table S5. *GAPDH* was used as a reference gene to normalize target gene expression.

2.7. Microarray Analysis

Microarray analyses, focused exclusively on a limited set of genes associated with lung development and the extracellular matrix, were performed on amniocytes, dermal fibroblasts, iPSCs, and organoids (d20-d60) using Affy Plus (Affymetrix, Santa Clara, CA). Lists of genes analyzed are shown in Table S2 and Table S3. Sample processing, probing to the Human Gene 2.1 ST array platform (Affymetrix), and data analysis were performed by the University of Michigan DNA Sequencing Core Microarray Facility. Normalized expressions by robust multiple-array averages were plotted using the heatmap.2 function from the gplots package in R (www.r-project.org) using default parameters. The euclidean distance dissimilarity matrix and complete linkage method were used to generate heatmap images. After exclusion of genes that were not present, values were normalized and compared to results from human fetal lung.[36]

2.8. Statistical Analysis

Quantitative analyses were presented as the mean±standard error of mean (SEM). Statistical comparisons were by the Mann-Whitney test or analysis of variance with Dunnett or Bonferroni correction for multiple comparisons, as appropriate, using GraphPad Prism software (version 8, GraphPad, La Jolla, CA). Results were considered to be statistically significant if $p \leq 0.05$. For immunostaining and qPCR of LOs, data were representative of at least three iPSC lines unless stated otherwise. Individual stainings and measurements were performed in triplicate. Additional details of statistical tests can be found in the Figure Legends.

3. Results

3.1. Generation of pluripotent stem cells from human congenital diaphragmatic hernia patients

We isolated human somatic cells from either the amniotic fluid (n=2) or foreskin (n=4) of children with CDH (Table S1). To epigenetically reprogram these cells into iPSCs, we used non-integrating Sendai virus (SeV). We confirmed that morphologically distinct CDH-iPSCs (Figure S1A, middle) expressed high levels of alkaline phosphatase comparable to those from embryonic stem cells (ESCs) and iPSCs derived from the same somatic tissue source in normal, non-CDH patients (Figure S1B). Between four and six weeks after exposure to SeV reprogramming factors, individual clones were mechanically picked and successfully transferred onto Matrigel-coated dishes for further

expansion, subculture, and additional characterization. Immunofluorescence staining revealed uniformly high expression of NANOG, OCT4, SOX2, and SSEA3 within colonies (Figure S1B). These data were supported by significant upregulation of pluripotency-specific genes, including *NANOG, OCT4, and SOX2*, in iPSC clones derived from CDH patients compared to those observed in respective parental somatic cells ($p \leq 0.01$, Figure S2C).

Cytogenetic analyses verified normal karyotypes, suggesting that CDH-iPSCs remained free from major non-clonal aberrations after continuous *in vitro* expansion for up to twenty passages (Figure S1C). To confirm that iPSC-CDH cells were capable of tri-lineage differentiation *in vitro*, CDH-iPSCs exhibited robust embryoid body formation as shown by the presence of derivatives from all three germ layers on immunohistochemistry (Figure S1D).

3.2. Human congenital diaphragmatic hernia induced pluripotent stem cells adopt fetal lung-like characteristics

We then exposed human iPSC-CDH clones to an established lung induction protocol (Figure 1A) based on manipulating fibroblast growth factor and hedgehog signaling as previously published.[31] Ventral-anterior foregut spheroids were generated from definitive endoderm in growth factor media containing FGF4, SAG, and CHIR99021, and subsequently cultured in Matrigel droplets. Spheroids grew robustly by

day 4 (Figure 1B), demonstrating typical patterned morphology.[31] Between 20 and 40 days of induction, ~30-35 organoids per well could be generated, each with multi-septated, sac-like architecture within the interior (Figure 1C). Organoid experiments were carried out for 20 (n=6), 40 (n=6), 60 (n=3), or 100 (n=1) days, and comparable results were obtained in each experiment using reprogrammed iPSCs clones from all six CDH patients (Table S1). The number of day-28 LOs was significantly decreased in CDH LOs compared to normal LOs (Figure 1D; 49.3± 7.0 vs. 114.6±11.2, respectively; $p \leq 0.01$), consistent with possible lung hypoplasia in CDH. To confirm directed differentiation of human iPSC-CDH clones into early LOs, we performed serial quantitative gene expression analyses at day 40 to determine degree of lung development. As expected, there were significant declines in *NANOG* and *OCT4* expression in CDH LOs and normal LOs (Figure 1E, $p \leq 0.01$).

We then conducted comparative analyses of normal and CDH LOs during the early lung differentiation phase by histology (Figure 2A), gene expression, and immunofluorescence. The expression of the lung/anterior foregut progenitor gene, *NKX2.1 (TTF-1),* was significantly upregulated in LOs at days 20 and 40, consistent with successful differentiation into the pulmonary lineage ($p \leq 0.01$; Figure 2B). Moreover, NKX2.1 protein expression was documented on confocal microscopy (Figure 2C) and was significantly increased in normal LOs compared with CDH LOs in quantitative analysis (Figure 2D, $p \leq 0.05$). Low or negligible expression of *PAX8*, a thyroid lineage

marker, in association with the LO induction protocol was confirmed (Figure 2E,F, $p \leq 0.01$). Demonstration of both epithelial and mesenchymal cell populations within normal and CDH LOs was shown by immunofluorescent staining for E-cadherin (Ecad) and α-smooth muscle actin/vimentin, respectively (Figure 2G).

The presence of type II alveolar cells, as suggested by surfactant protein-C (SFTPC) protein expression, was evident adjacent to $NKX2.1^+$ cells by day 20 (Figure 2H,I, $p \leq 0.01$). The presence of type I epithelial cells was supported by podoplanin (PDPN) staining in an alveolar-like distribution along the periphery of cells in both normal and CDH LOs (Figure 2J). Furthermore, LOs showed significant downregulation of the endodermal gene, *FOXA2,* as well as a significant upregulation of the lung epithelial genes, *AQP5 and SFTPC* ($p \leq 0.05$ and $p \leq 0.01$, respectively; Figure 2K). The mesenchymal gene, vimentin (*VIM*), was also significantly upregulated during LO induction ($p \leq 0.01$). Taken together, these results were consistent with the successful differentiation of pluripotent stem cells from CDH patients into multicellular LOs containing both pulmonary epithelial and mesenchymal derivatives.

To further assess proximal and distal airway progenitor cell differentiation within LOs, we then systematically analyzed LOs at day 40. There was intermittent but robust SFTPC staining throughout the periphery of cells (Figure 3A). Co-localization of $SFTPC^+$ and $SOX9^+$ cells was evident, supporting the differentiation of distal pulmonary epithelial cell types. Quantitative protein counts at day 40 confirmed significant

decreases in SFTPC expression in CDH LOs compared to counts in normal LOs (Figure 3B, p≤0.01). Double staining of LO sections showed the presence of the basal bronchial marker, p63, adjacent to cells with PDPN peripheral enhancement (Figure 3C). Previous work using this same induction protocol has shown that $p63^+$ cells possess an $NKX2.1^+$ identity.[31] There were no significant differences in p63 and PDPN expression between normal and CDH LOs (Figure 3D,E).

3.3. Targeted microarray analyses reveal upregulation in extracellular matrix gene expression within human CDH lung organoids

To assess for similarities and differences in gene expression between CDH-LOs and control LOs during organoid differentiation, we performed a microarray analysis using panels targeting genes associated with lung development and extracellular matrix (ECM) activity (Tables S2 and S3, respectively). After normalization of gene expression relative to parental iPSCs, heatmaps of upregulated and downregulated genes in day-20, -40, and -60 CDH LOs were generated and compared to age-matched normal LOs (Figure 3F,G). Volcano plots of differentially expressed lung development-associated genes in day-40 CDH LOs revealed significant dysregulation in only two (1.9%) genes, fibroblast growth factor-18 (*FGF18*) and cysteine rich secretory protein LCCL domain containing-2 (*CRISPLD2*), relative to day-40 normal LOs (Figure 3H, >2-fold change, p≤0.05). No significant dysregulation was seen in day-20 or day-60 CDH LOs.

Moreover, there were no differentially expressed genes associated with lung development, including markers of retinoic acid signaling (*STRA6*, *RBP4*), among CDH LOs evaluated (volcano plots not shown). Sonic hedgehog (*SHH*) was downregulated in day-40 CDH LOs, but this did not meet statistical significance (p=0.058). In contrast, there were fifteen (10.9%) ECM-associated genes that were significantly upregulated in day-40 CDH LOs (Figure 3I), including hyaluronan and proteoglycan link protein-1 (*HAPLN1*), aggrecan (*ACAN*), and elastin microfibril interface-1 (*EMILIN1*, >2-fold change, p≤0.05).

3.4. Human CDH lung organoids show impairments in pulmonary epithelial and mesenchymal differentiation

We also performed a comparative analysis of proximal and distal lung gene expression within normal and CDH LOs up to day 60 of lung differentiation. High gene expression of the proximal lung progenitor marker, *SOX2,* was maintained in iPSC-LO clones from both CDH and normal patients for up to 60 days after induction but was significantly diminished in day-60 CDH LOs (Figure 4A, top; p≤0.01). There was significant upregulation of the distal lung progenitor marker, *SOX9,* among LOs compared to that observed in baseline parental iPSCs (p≤0.01). However, gene expression of *SOX9* was significantly lower at day 60 in CDH LOs compared to LOs derived from children with normal lungs (Figure 4A, middle; p≤0.01). *NKX2.1* gene

expression remained significantly impaired in day-60 CDH LOs (Figure 4A, bottom; $p \leq 0.01$). Taken together, these data suggest possible impairment in the differentiation of human CDH-LOs into NKX2.1$^+$, SOX2$^+$, and SOX9$^+$ progenitors under identical conditions, even in the absence of mechanical compression.

We then directly compared how markers of pulmonary differentiation within human CDH-LOs might differ from those in human perinatal lung tissue. Confocal microscopy images of CDH LOs exhibited similar lung progenitor cell immunostaining patterns comparable to those observed in infant CDH lung, including NKX2.1$^+$ lung progenitors and endodermal SOX17$^+$ cells (Figure 4B). In other areas adjacent to hollow lumen-like structures, there was a robust staining for Ecad and a relative paucity of NKX2.1$^+$ cells compared to that observed in native lung tissue and normal LO controls.

We also evaluated differences in proliferating cells within CDH LOs compared to normal LO controls. Expression of *Ki67*, a cellular proliferation gene, was maintained in all iPSCs throughout the LO induction phase (Figure 4C), but significant reductions were observed at later timepoints ($p \leq 0.01$). There were no significant differences in *Ki67* gene expression between LOs from normal iPSCs and those derived from iPSCs-CDH. Confocal sections demonstrated microscopic luminal structures lined with SFTPC$^+$ cells and Ki67$^+$ cells along the basal region (Figure 4D, top). There was scant evidence of the cellular apoptosis protein, activated caspase-3 (Cas3), in normal and CDH lung organoids by immunofluorescence staining (Figure 4D, bottom).

We further characterized specific pulmonary epithelial and mesenchymal cell phenotypes in day-40 and day-60 CDH LOs by serial quantitative RT-PCR. We measured two type II lung epithelial markers, namely surfactant protein-B (*SFTPB*) and *SFTPC*, and found significantly lower expression of both genes in CDH LOs (Figure 5A, $p \leq 0.01$). HOPX and PDPN were also evaluated and were significantly elevated to comparable levels compared to parental iPSCs in both normal and CDH LOs.

Pulmonary differentiation of CDH LOs into specific epithelial subtypes was shown by confocal microscopy, displaying numerous proximal lung progenitor cell types by day 40 (Figure 5B). There were multiple proximal airway subtypes, as shown by positive acetylated alpha-tubulin (ciliated), MUC5b (goblet), PLUNC (secretory), p63, and club cell secretory protein (CCSP) staining. Staining of the stromal compartment within CDH LOs revealed well-organized PDGFRα^+/VIM$^+$ myofibroblasts along the periphery of lumen-like structures (Figure 5C).

Serial quantitative gene expression data of normal and CDH LOs revealed upregulation of *VIM*, *αSMA*, and *PDGFRα* (Figure 5D). However, whereas levels of expression of *VIM* and *αSMA* were similar between normal and CDH LOs, there was significantly decreased expression of *PDGFRα* in CDH LOs tested at both day 40 and day 60 ($p \leq 0.01$). Taken together, these results suggest possible differences in type II alveolar epithelial cell and PDGFRα-related differentiation among CDH LOs in the absence of mechanical compression forces.

3.5. Ex vivo mechanical compression alters human CDH lung organoid development

To study the contribution that extrinsic compression may play in the development of the CDH lung phenotype, we used an *ex vivo* mechanical compression apparatus as previously described[33,34] and tested its effect on day-40 LOs that were otherwise cultured under the same growth conditions (Figure 6A). This time point was chosen since LOs differentiation was analogous to the pseudoglandular stage of lung development based on previous work.[31,37] In an effort to mimic *in utero* mechanical forces in fetal CDH, 100 (1.4 cm H_2O), 200 (2.7 cm H_2O), or 400 (5.4 cm H_2O) Pa of static compression forces were used.

Although gross inspection was notable for obvious flattening of the organoid tissue after compression, confocal microscopy images showed no obvious micro-architectural differences by hematoxylin and eosin (H&E) staining (Figure 6B, left). Evidence of Ki67/Cas3 immunofluorescent staining suggested ongoing cell proliferation and apoptosis (Figure 6B, middle). There was significant gene downregulation in *PDPN* (at 400 Pa only) and *Ki67*, suggesting an overall reduction in organoid cell proliferation caused by the compression stimulus (Figure 6C, $p \leq 0.01$). CDH-specific alterations in gene expression under increased mechanical compression were demonstrated by significant reduction in *NKX2.1* (Figure 6D, $p \leq 0.01$), and upregulation in *FOXA2* (Figure

6D, p≤0.01) and *VIM* (Figure 6E, p≤0.01) with escalating pressures. In contrast, there was specific and significant upregulation in *NKX2.1* in normal LOs with mechanical compression (Figure 6D, p≤0.01).

In parallel with these findings, there was significant stepwise downregulation in the expression of lung progenitor genes, *SOX2* and *SOX9,* (Figure 7A) in both CDH and normal LOs at higher pressures (p≤0.01). Increased NKX2.1 in response in mechanical compression among normal LOs was supported by immunofluorescence (Figure 7B) and shown by quantitative protein expression (Figure 7C). Compression was associated with reduced SOX9 protein expression that was specific to CDH LOs (Figure 7D). Confocal images revealed evidence for increased VIM expression within the cytoplasm of CDH LOs (Figure 7E), although these levels could not be formally quantified. Combined, these data lend support to the concept of disease- and cell phenotype-specific changes in response to mechanical compression in CDH, resulting in altered progenitor, epithelial, and mesenchymal cell development within the developing lung.

4. Discussion

CDH is a perplexing congenital lung anomaly whose exact cause remains unknown.[38] Although somatic mutations in *GATA4 and FOG2,* among others, have been implicated in less than ten percent of CDH patients,[15,16,39] the etiology of CDH is heterogeneous and likely polygenic in the majority of cases.[12] Regardless, the

downstream result of the near-term CDH fetal lung is progressive hypoplasia involving both proximal and distal airways as well as abnormalities within the adjacent mesenchyme and airway smooth muscle.[21,40] At autopsy in both CDH fetuses and infants, pathologic evaluation of the lung uniformly reveals a spectrum of developmental abnormalities, including impairments in alveolarization, decreased vascularization, and smooth muscle arteriole hypertrophy.[40-42] The ability to elucidate the mechanisms of disease contributing to these lung derangements has been mixed despite decades of animal model research.[43,44]

In this study, we report on the directed differentiation of human iPSCs derived from CDH amniotic fluid and neonatal skin into 3D fetal lung-like structures using an established and highly reproducible protocol.[32] In addition to previous work demonstrating the presence of gene, protein, and electron microscopy data on distal lung differentiation, bulk RNA-seq analyses have shown that organoids from non-CDH patients produced by this method are more similar to native fetal lung than to adult lung.[31] We then subjected our CDH LOs to *ex vivo* mechanical forces to evaluate the contribution of pathologic compression on pulmonary development. Although the role of mechanical strain on lung epithelia in 2D culture has been studied by others to understand mechanisms of ventilator-associated lung injury and other acquired pathologies,[45,46] the role of mechanical factors on multicellular human organoids has not been explored in an *ex vivo* setting. Here, by simulating what would occur when the

CDH fetal lung becomes physically constrained by space-occupying abdominal organs within the pleural space, we observed a reproducible and stepwise downregulation in the expression of lung progenitor genes, *SOX2* and *SOX9,* with increasing mechanical pressures (Figure 7). There was also a profound decrease in *NKX2.1* and *PDPN* gene expression along with an increase in *FOXA2* and *VIM* gene expression in CDH LOs (Figure 6), reflecting the differential effects of mechanical forces on distinct cell types within developing organoids. ne

Lack of NKX2.1^{+} cells within the developing lung has been associated with loss of type I pneumocytes and perinatal tissue damage,[47,48] whereas upregulation of *FOXA2* has been shown to correlate with proximal airway epithelial cell and type II alveolar proliferation.[49] The negative effect of mechanical compression on *PDPN*, a gene expressed in gas-exchanging (type I) pneumocytes, is not trivial since these cells cover 95% of the alveolar surface of the lung[50] and was recently confirmed to be markedly diminished in a murine model of CDH.[51] In contrast, type II pneumocytes serve as alveolar stem cells and secrete pulmonary surfactant.[52] The increased expression of *VIM* is consistent with a pro-fibroblastic response in setting of an non-physiological mechanical stimulus.[53] Taken together, since we were able to quantitatively apply disease relevant compression forces to our CDH LOs roughly corresponding to the pseudoglandular and early canalicular stages of development,

these findings suggest a new *in vitro* research platform to study the mechanobiology and patient-specific disease pathogenesis of human CDH fetal lung hypoplasia.

Although mechanical pressure gradients play an important and essential role in regulating normal lung morphogenesis,[54-56] the role of *NKX2.1* in normal and CDH lung development remains relatively unknown.[57] The fetus itself is known to initiate "breathing" movements, where amniotic fluid is intermittently inhaled and exhaled starting during the canalicular stage of pulmonary development.[58-60] It has also been shown that there are spontaneous peristaltic airway contractions within the fetal lung that can propel lung liquid through the bronchial tree.[61] Using embryonic murine lung explants within bioengineered microfluidic devices, increased transmural pressures can accelerate the rate of airway epithelial morphogenesis due to crosstalk between different tissues.[17] The strategy to induce lung growth in CDH through the augmentation of transmural (intrapulmonary) pressures has already been applied experimentally in humans by fetoscopic tracheal occlusion (FETO), a procedure performed at our hospital and other selected fetal care centers worldwide.[4,62] During FETO-induced lung growth in experimental models, a marked proliferation of type I alveolar epithelial cells, potentially involving the FGF10-FGFR2b-Sprouty2 pathway, has been shown.[63,64] FETO does not appear to increase NKX2.1 expression in either normal or CDH fetal lungs in late gestational animal models.[63,65]

Despite the lack of contiguous airway branching structures within our 3D LOs, we mimicked the low intrapulmonary transmural pressures seen clinically in CDH by applying external mechanical forces in an *ex vivo* system. We found an overall reduction in cell proliferation using *Ki67* (Figure 5A) as well as impaired expression of *NKX2.1* and *PDPN* (Figure 5D). Our data are also concordant with previous work based on our *ex vivo* compression apparatus used to assess changes in fetal rat lungs.[34] In that study, we found that mechanical compression impaired normal lung growth based on branching morphometric analyses but did not significantly alter surfactant protein or α*SMA* gene expression.

Perhaps the most intriguing observation in our study is the data suggesting an inherent impairment in LO development in CDH patients, even in the absence of mechanical compression forces. Compared with LOs derived from normal, non-CDH patients cultured under identical conditions, the differentiation of CDH LOs was associated with impaired *NKX2.1*, *SOX2*, *SOX9*, *SFTPB, SFTPC,* and *PDGFR*α expression under routine conditions. PDGFRα, a tyrosine kinase receptor expressed by alveolar myofibroblasts, has been shown to be critical for early lung branching and alveolarization.[66,67] Approximately ten percent of ECM-related genes, many associated with proximal/bronchial airway formation, were significantly upregulated in day-40 CDH LOs in microarray analyses (Figure 3D). Collectively, these findings support the concept of CDH as a global embryopathy,[68] which argues that a more basic, mesenchymal cell-

intrinsic disturbance during early fetal development may exist in these patients, leading to pleiotropic effects on the lung and adjacent diaphragm.[12,21,69] In fetal rodent models of CDH lung hypoplasia, global embryopathy as a cause of CDH has been supported by observations of abnormal branching morphogenesis that precedes normal formation of the diaphragm as early as E11.[25,70] Moreover, there is always lung hypoplasia in these models despite the fact that approximately half of fetal pups never develop the diaphragmatic hernia itself.[71] Although experimental work in our laboratory [72] has also shown that hypoplastic fetal lungs in the nitrofen rat model of CDH undergo some catchup lung growth when explanted and cultured *ex vivo* in the absence of compression forces, others have observed persistent hypoplasia under similar conditions.[73]

Given the findings in our study, the application of mechanical compression may represent a “second hit” in which lung hypoplasia is further aggravated, perhaps by aberrant mesenchymal-epithelial responses to compression stimuli as we and others have previously suggested in rodent models.[22,34] Some experimental evidence supports an underlying dysfunction in mesenchymal cells associated with defective alveolarization in CDH.[74-76] Investigators have also shown that soluble factors secreted by the mesenchyme can have effects on alveolar progenitor cell differentiation.[77] Others have found that PDGFRα-expressing cells within the mesenchyme migrate to the tips of secondary alveolar septa and differentiate into α-actin- and elastin-producing

myofibroblasts that are required for normal alveolar development and gas exchange.[66,67,78] We speculate that PDGFRα^+ cells in CDH may be impaired in many patients, resulting in subsequent downstream effects on early lung branching and alveolarization.[79] The lack of significant changes in *αSMA* gene expression, a general marker of smooth muscle cells, among CDH LOs when compared to control LOs is discordant with nitrofen rat studies[80] but is consistent with recent autopsy reports conducted in term CDH infants.[81]

Reduced expression of *SHH* during the pseudoglandular phase of lung development has been implicated in the nitrofen model.[82] Our microarray data also revealed decreased *SHH* expression in day-40 CDH LOs, but this narrowly missed statistical significance. Although we found evidence for increased ECM gene expression in CDH LOs (Figure 3G), evaluation using RNA-seq technology would be instrumental towards gaining a better understanding of the genes and molecular regulatory networks involved in mediating early lung development with or without the presence of mechanical forces. Previous studies on transcriptome profiling of human fetal lungs are now readily available.[37] The role of *FOXA2* in CDH and whether patients with a more severe CDH phenotype have more intrinsic derangements during LO differentiation remain unknown and are currently under investigation in our laboratory.

Despite the promising data presented in this study, there are notable limitations to this work. First, the creation of 3D LOs from human iPSCs requires months and

remains labor intensive. As a result, we studied the effect of one type of mechanical compression at one specific time point in CDH organoid differentiation. It is likely that the application of various types of mechanical forces, such as intermittent compression or chronic compression, may induce unique and different time-dependent effects on organoid differentiation.[17,83] Second, further work is needed using additional CDH and normal control samples given that CDH is a polygenic disorder across a wide disease spectrum, and there are likely to be additional variations in the differentiation capabilities of various iPSC clones, which is beyond the scope of our study. There are more than 20 different genetic mutations that have been described in non-syndromic CDH, and a laboratory gene panel does not currently exist to screen for these genes.[10] Third, it is possible that alternative directed differentiation protocols, as we and others have described,[84-86] may yield different results within our *ex vivo* compression system. Fourth, unlike hypoplastic fetal rodent lung explants used in our laboratory and elsewhere,[72] this organoid model is not suitable for studying aberrant CDH branching morphogenesis[85] and the subsequent instructional role that airway smooth muscle may play during this process.[87] Finally, it is difficult to evaluate function in LOs, and we cannot evaluate morphometric aspects of LOs, such size and complexity, as well as other components of lung development including pulmonary blood vessel formation, an important aspect in CDH lung development.[88,89] Studies of the latter would likely require the *in vivo* transfer

of LOs as our laboratory and others have previously described using LOs derived from non-CDH patients.[90,91]

5. Conclusion

In this proof of concept paper, we describe a stem cell-based approach to facilitate the study of disease pathogenesis in CDH fetal lung hypoplasia. Ongoing studies using these CDH organoids should allow us to better understand epithelial-mesenchymal cell interactions that occur early in this unique disease-specific microenvironment.[77] Further advancement of this translational work will also represent the necessary steps towards developing cell-based therapies and the testing of experimental pharmacologic agents, including pulmonary morphogens and growth factors,[92-94] as potential approaches to enhance perinatal lung development and differentiation in these fragile children.

Acknowledgments

The authors thank Jeannie Kreutzman, RN, MSN, CPNP, for facilitating the collection of amniotic fluid specimens, as well as Craig Johnson at the University of Michigan for their assistance with the microarray analysis. S.M.K. was funded by the Department of Surgery and philanthropic sources from the University of Michigan and Johns Hopkins University. J.R.S. is supported by the NIH-NHLBI (R01 HL119215).

Conflict of Interest

The authors indicated no potential conflicts of interest.

Data Availability Statement

The data used to support the findings of this study are available from the corresponding author upon request.

References

1. Putnam LR, Harting MT, Tsao K, et al. Congenital Diaphragmatic Hernia Defect Size and Infant Morbidity at Discharge. *Pediatrics.* 2016;138.
2. Cameron DB, Graham DA, Milliren CE, et al. Quantifying the Burden of Interhospital Cost Variation in Pediatric Surgery: Implications for the Prioritization of Comparative Effectiveness Research. *JAMA Pediatr.* 2017;171:e163926.
3. Kays DW, Islam S, Larson SD, et al. Long-term Maturation of Congenital Diaphragmatic Hernia Treatment Results Toward Development of a Severity-Specific Treatment Algorithm. *Annals of Surgery.* 2013;258:638-645.
4. Harrison MR, Keller RL, Hawgood SB, et al. A randomized trial of fetal endoscopic tracheal occlusion for severe fetal congenital diaphragmatic hernia. *N Engl J Med.* 2003;349:1916-1924.
5. Kunisaki SM, Barnewolt CE, Estroff JA, et al. Ex utero intrapartum treatment with extracorporeal membrane oxygenation for severe congenital diaphragmatic hernia. *J Pediatr Surg.* 2007;42:98-104; discussion 104-106.
6. Harting MT, Hollinger L, Tsao K, et al. Aggressive Surgical Management of Congenital Diaphragmatic Hernia: Worth the Effort?: A Multicenter, Prospective, Cohort Study. *Ann Surg.* 2018;267:977-982.

7. Muratore CS, Kharasch V, Lund DP, et al. Pulmonary morbidity in 100 survivors of congenital diaphragmatic hernia monitored in a multidisciplinary clinic. *J Pediatr Surg.* 2001;36:133-140.

8. Dao DT, Hayden LP, Buchmiller TL, et al. Longitudinal Analysis of Pulmonary Function in Survivors of Congenital Diaphragmatic Hernia. *The Journal of pediatrics.* 2019.

9. Rottier R, Tibboel D. Fetal lung and diaphragm development in congenital diaphragmatic hernia. *Semin Perinatol.* 2005;29:86-93.

10. Yu L, Hernan RR, Wynn J, et al. The influence of genetics in congenital diaphragmatic hernia. *Semin Perinatol.* 2019:151169.

11. Wynn J, Yu L, Chung WK. Genetic causes of congenital diaphragmatic hernia. *Semin Fetal Neonatal Med.* 2014;19:324-330.

12. Ameis D, Khoshgoo N, Keijzer R. Abnormal lung development in congenital diaphragmatic hernia. *Semin Pediatr Surg.* 2017;26:123-128.

13. Russell MK, Longoni M, Wells J, et al. Congenital diaphragmatic hernia candidate genes derived from embryonic transcriptomes. *Proc Natl Acad Sci U S A.* 2012;109:2978-2983.

14. Veenma DC, de Klein A, Tibboel D. Developmental and genetic aspects of congenital diaphragmatic hernia. *Pediatr Pulmonol.* 2012;47:534-545.

15. Ackerman KG, Herron BJ, Vargas SO, et al. Fog2 is required for normal diaphragm and lung development in mice and humans. *PLoS Genet.* 2005;1:58-65.

16. Yu L, Wynn J, Cheung YH, et al. Variants in GATA4 are a rare cause of familial and sporadic congenital diaphragmatic hernia. *Hum Genet.* 2013;132:285-292.

17. Nelson CM, Gleghorn JP, Pang MF, et al. Microfluidic chest cavities reveal that transmural pressure controls the rate of lung development. *Development.* 2017;144:4328-4335.

18. Wells LJ. A study of closure of the pleuropericardial and pleuroperitoneal canals in the human embryo. *Anat Rec.* 1947;97:428.

19. Harrison MR, Jester JA, Ross NA. Correction of congenital diaphragmatic hernia in utero. I. The model: intrathoracic balloon produces fatal pulmonary hypoplasia. *Surgery.* 1980;88:174-182.

20. Lazar DA, Ruano R, Cass DL, et al. Defining "liver-up": does the volume of liver herniation predict outcome for fetuses with isolated left-sided congenital diaphragmatic hernia? *J Pediatr Surg.* 2012;47:1058-1062.

21. Jesudason EC. Small lungs and suspect smooth muscle: congenital diaphragmatic hernia and the smooth muscle hypothesis. *J Pediatr Surg.* 2006;41:431-435.

22. Keijzer R, Liu J, Deimling J, et al. Dual-hit hypothesis explains pulmonary hypoplasia in the nitrofen model of congenital diaphragmatic hernia. *Am J Pathol.* 2000;156:1299-1306.

23. Jesudason EC, Losty PD, Lloyd DA. Pulmonary hypoplasia: alternative pathogenesis and antenatal therapy in diaphragmatic hernia. *Archives of disease in childhood Fetal and neonatal edition.* 2000;82:F172.

24. Derderian SC, Jayme CM, Cheng LS, et al. Mass Effect Alone May Not Explain Pulmonary Vascular Pathology in Severe Congenital Diaphragmatic Hernia. *Fetal Diagn Ther.* 2016;39:117-124.

25. Guilbert TW, Gebb SA, Shannon JM. Lung hypoplasia in the nitrofen model of congenital diaphragmatic hernia occurs early in development. *Am J Physiol Lung Cell Mol Physiol.* 2000;279:L1159-1171.

26. Correia-Pinto J, Baptista MJ, Pedrosa C, et al. Fetal heart development in the nitrofen-induced CDH rat model: the role of mechanical and nonmechanical factors. *J Pediatr Surg.* 2003;38:1444-1451.

27. Jay PY, Bielinska M, Erlich JM, et al. Impaired mesenchymal cell function in Gata4 mutant mice leads to diaphragmatic hernias and primary lung defects. *Dev Biol.* 2007;301:602-614.

28. Jiang G, Di Bernardo J, Maiden MM, et al. Human transgene-free amniotic-fluid-derived induced pluripotent stem cells for autologous cell therapy. *Stem Cells Dev.* 2014;23:2613-2625.

29. Jiang G, Herron TJ, Di Bernardo J, et al. Human Cardiomyocytes Prior to Birth by Integration-Free Reprogramming of Amniotic Fluid Cells. *Stem cells translational medicine.* 2016;5:1595-1606.

30. Itskovitz-Eldor J, Schuldiner M, Karsenti D, et al. Differentiation of human embryonic stem cells into embryoid bodies compromising the three embryonic germ layers. *Mol Med.* 2000;6:88-95.

31. Dye BR, Hill DR, Ferguson MA, et al. In vitro generation of human pluripotent stem cell derived lung organoids. *Elife.* 2015;4.

32. Miller AJ, Dye BR, Ferrer-Torres D, et al. Generation of lung organoids from human pluripotent stem cells in vitro. *Nat Protoc.* 2019;14:518-540.

33. Tse JM, Cheng G, Tyrrell JA, et al. Mechanical compression drives cancer cells toward invasive phenotype. *Proc Natl Acad Sci U S A.* 2012;109:911-916.

34. Fox ZD, Jiang G, Ho KKY, et al. Fetal lung transcriptome patterns in an ex vivo compression model of diaphragmatic hernia. *The Journal of surgical research.* 2018;231:411-420.

35. Olver RE, Walters DV, S MW. Developmental regulation of lung liquid transport. *Annu Rev Physiol.* 2004;66:77-101.

36. Huang DW, Sherman BT, Tan Q, et al. The DAVID Gene Functional Classification Tool: a novel biological module-centric algorithm to functionally analyze large gene lists. *Genome Biol.* 2007;8:R183.

37. Kho AT, Bhattacharya S, Tantisira KG, et al. Transcriptomic analysis of human lung development. *Am J Respir Crit Care Med.* 2010;181:54-63.

38. Kool HM, Burgisser PE, Edel GG, et al. Inhibition of retinoic acid signaling induces aberrant pericyte coverage and differentiation resulting in vascular defects in congenital diaphragmatic hernia. *Am J Physiol Lung Cell Mol Physiol.* 2019;317:L317-L331.

39. Yu L, Wynn J, Ma L, et al. De novo copy number variants are associated with congenital diaphragmatic hernia. *J Med Genet.* 2012;49:650-659.

40. Bargy F, Beaudoin S, Barbet P. Fetal lung growth in congenital diaphragmatic hernia. *Fetal Diagn Ther.* 2006;21:39-44.

41. Kitagawa M, Hislop A, Boyden EA, et al. Lung hypoplasia in congenital diaphragmatic hernia. A quantitative study of airway, artery, and alveolar development. *The British journal of surgery.* 1971;58:342-346.

42. Heerema AE, Rabban JT, Sydorak RM, et al. Lung pathology in patients with congenital diaphragmatic hernia treated with fetal surgical intervention, including tracheal occlusion. *Pediatr Dev Pathol.* 2003;6:536-546.

43. Nakao Y, Ueki R. Congenital diaphragmatic hernia induced by nitrofen in mice and rats: Characteristics as animal model and pathogenetic relationship between diaphragmatic hernia and lung hypoplasia. *Congenital Anomalies.* 1987;27:397-417.

44. van Loenhout RB, Tibboel D, Post M, et al. Congenital diaphragmatic hernia: comparison of animal models and relevance to the human situation. *Neonatology.* 2009;96:137-149.

45. Waters CM, Roan E, Navajas D. Mechanobiology in lung epithelial cells: measurements, perturbations, and responses. *Compr Physiol.* 2012;2:1-29.

46. Sanchez-Esteban J, Wang Y, Cicchiello LA, et al. Cyclic mechanical stretch inhibits cell proliferation and induces apoptosis in fetal rat lung fibroblasts. *Am J Physiol Lung Cell Mol Physiol.* 2002;282:L448-456.

47. Herriges MJ, Tischfield DJ, Cui Z, et al. The NANCI-Nkx2.1 gene duplex buffers Nkx2.1 expression to maintain lung development and homeostasis. *Genes Dev.* 2017;31:889-903.

48. Little DR, Gerner-Mauro KN, Flodby P, et al. Transcriptional control of lung alveolar type 1 cell development and maintenance by NK homeobox 2-1. *Proc Natl Acad Sci U S A.* 2019;116:20545-20555.

49. Wan H, Dingle S, Xu Y, et al. Compensatory roles of Foxa1 and Foxa2 during lung morphogenesis. *J Biol Chem.* 2005;280:13809-13816.

50. Stone KC, Mercer RR, Gehr P, et al. Allometric relationships of cell numbers and size in the mammalian lung. *Am J Respir Cell Mol Biol.* 1992;6:235-243.

51. Nguyen TM, Jimenez J, Rendin LE, et al. The proportion of alveolar type 1 cells decreases in murine hypoplastic congenital diaphragmatic hernia lungs. *PLoS One.* 2019;14:e0214793.

52. Barkauskas CE, Cronce MJ, Rackley CR, et al. Type 2 alveolar cells are stem cells in adult lung. *J Clin Invest.* 2013;123:3025-3036.

53. Kuhn H, Zobel C, Vollert G, et al. High amplitude stretching of ATII cells and fibroblasts results in profibrotic effects. *Exp Lung Res.* 2019;45:167-174.

54. Kitterman JA. The effects of mechanical forces on fetal lung growth. *Clin Perinatol.* 1996;23:727-740.

55. Nicolini U, Fisk NM, Rodeck CH, et al. Low amniotic pressure in oligohydramnios--is this the cause of pulmonary hypoplasia? *Am J Obstet Gynecol.* 1989;161:1098-1101.

56. Varner VD, Gleghorn JP, Miller E, et al. Mechanically patterning the embryonic airway epithelium. *Proc Natl Acad Sci U S A.* 2015;112:9230-9235.

57. Inanlou MR, Baguma-Nibasheka M, Kablar B. The role of fetal breathing-like movements in lung organogenesis. *Histol Histopathol.* 2005;20:1261-1266.

58. Nobuhara KK, Wilson JM. The effect of mechanical forces on in utero lung growth in congenital diaphragmatic hernia. *Clin Perinatol.* 1996;23:741-752.

59. Koos BJ, Rajaee A. Fetal breathing movements and changes at birth. *Adv Exp Med Biol.* 2014;814:89-101.

60. Jesudason EC, Smith NP, Connell MG, et al. Developing rat lung has a sided pacemaker region for morphogenesis-related airway peristalsis. *Am J Respir Cell Mol Biol.* 2005;32:118-127.

61. Schittny JC, Miserocchi G, Sparrow MP. Spontaneous peristaltic airway contractions propel lung liquid through the bronchial tree of intact and fetal lung explants. *Am J Respir Cell Mol Biol.* 2000;23:11-18.

62. Seravalli V, Jelin EB, Miller JL, et al. Fetoscopic tracheal occlusion for treatment of non-isolated congenital diaphragmatic hernia. *Prenat Diagn.* 2017;37:1046-1049.

63. Chapin CJ, Ertsey R, Yoshizawa J, et al. Congenital diaphragmatic hernia, tracheal occlusion, thyroid transcription factor-1, and fetal pulmonary epithelial maturation. *Am J Physiol Lung Cell Mol Physiol.* 2005;289:L44-52.

64. Unbekandt M, del Moral PM, Sala FG, et al. Tracheal occlusion increases the rate of epithelial branching of embryonic mouse lung via the FGF10-FGFR2b-Sprouty2 pathway. *Mech Dev.* 2008;125:314-324.

65. Danzer E, Robinson LE, Davey MG, et al. Tracheal occlusion in fetal rats alters expression of mesenchymal nuclear transcription factors without affecting surfactant protein expression. *J Pediatr Surg.* 2006;41:774-780.

66. Ntokou A, Klein F, Dontireddy D, et al. Characterization of the platelet-derived growth factor receptor-alpha-positive cell lineage during murine late lung development. *Am J Physiol Lung Cell Mol Physiol.* 2015;309:L942-958.

67. Endale M, Ahlfeld S, Bao E, et al. Temporal, spatial, and phenotypical changes of PDGFRalpha expressing fibroblasts during late lung development. *Dev Biol.* 2017;425:161-175.

68. Molenaar JC, Bos AP, Hazebroek FW, et al. Congenital diaphragmatic hernia, what defect? *J Pediatr Surg.* 1991;26:248-254.

69. Clugston RD, Zhang W, Greer JJ. Gene expression in the developing diaphragm: significance for congenital diaphragmatic hernia. *Am J Physiol Lung Cell Mol Physiol.* 2008;294:L665-675.

70. Featherstone NC, Connell MG, Fernig DG, et al. Airway smooth muscle dysfunction precedes teratogenic congenital diaphragmatic hernia and may contribute to hypoplastic lung morphogenesis. *Am J Respir Cell Mol Biol.* 2006;35:571-578.

71. Montalva L, Zani A. Assessment of the nitrofen model of congenital diaphragmatic hernia and of the dysregulated factors involved in pulmonary hypoplasia. *Pediatr Surg Int.* 2019;35:41-61.

72. Di Bernardo J, Maiden MM, Hershenson MB, et al. Amniotic fluid derived mesenchymal stromal cells augment fetal lung growth in a nitrofen explant model. *J Pediatr Surg.* 2014;49:859-865.

73. Leinwand MJ, Tefft JD, Zhao J, et al. Nitrofen inhibition of pulmonary growth and development occurs in the early embryonic mouse. *J Pediatr Surg.* 2002;37:1263-1268.

74. van Loenhout RB, Tseu I, Fox EK, et al. The pulmonary mesenchymal tissue layer is defective in an in vitro recombinant model of nitrofen-induced lung hypoplasia. *Am J Pathol.* 2012;180:48-60.

75. Costlow RD, Manson JM. The heart and diaphragm: target organs in the neonatal death induced by nitrofen (2,4-dichlorophenyl-p-nitrophenyl ether). *Toxicology.* 1981;20:209-227.

76. Donahoe PK, Longoni M, High FA. Polygenic Causes of Congenital Diaphragmatic Hernia Produce Common Lung Pathologies. *Am J Pathol.* 2016;186:2532-2543.

77. Leeman KT, Pessina P, Lee JH, et al. Mesenchymal Stem Cells Increase Alveolar Differentiation in Lung Progenitor Organoid Cultures. *Sci Rep.* 2019;9:6479.

78. Deimling J, Thompson K, Tseu I, et al. Mesenchymal maintenance of distal epithelial cell phenotype during late fetal lung development. *Am J Physiol Lung Cell Mol Physiol.* 2007;292:L725-741.

79. Kotecha S. Lung growth: implications for the newborn infant. *Archives of disease in childhood Fetal and neonatal edition.* 2000;82:F69-74.

80. Coleman C, Zhao J, Gupta M, et al. Inhibition of vascular and epithelial differentiation in murine nitrofen-induced diaphragmatic hernia. *Am J Physiol.* 1998;274:L636-646.

81. Sluiter I, van der Horst I, van der Voorn P, et al. Premature differentiation of vascular smooth muscle cells in human congenital diaphragmatic hernia. *Exp Mol Pathol.* 2013;94:195-202.

82. Unger S, Copland I, Tibboel D, et al. Down-regulation of sonic hedgehog expression in pulmonary hypoplasia is associated with congenital diaphragmatic hernia. *Am J Pathol.* 2003;162:547-555.

83. Bougault C, Paumier A, Aubert-Foucher E, et al. Molecular analysis of chondrocytes cultured in agarose in response to dynamic compression. *BMC Biotechnol.* 2008;8:71.

84. Miller AJ, Hill DR, Nagy MS, et al. In Vitro Induction and In Vivo Engraftment of Lung Bud Tip Progenitor Cells Derived from Human Pluripotent Stem Cells. *Stem Cell Reports.* 2018;10:101-119.

85. Chen YW, Huang SX, de Carvalho A, et al. A three-dimensional model of human lung development and disease from pluripotent stem cells. *Nat Cell Biol.* 2017;19:542-549.

86. Leibel SL, Winquist A, Tseu I, et al. Reversal of Surfactant Protein B Deficiency in Patient Specific Human Induced Pluripotent Stem Cell Derived Lung Organoids by Gene Therapy. *Sci Rep.* 2019;9:13450.

87. Pieretti AC, Ahmed AM, Roberts JD, Jr., et al. A novel in vitro model to study alveologenesis. *Am J Respir Cell Mol Biol.* 2014;50:459-469.

88. Muehlethaler V, Kunig AM, Seedorf G, et al. Impaired VEGF and nitric oxide signaling after nitrofen exposure in rat fetal lung explants. *Am J Physiol Lung Cell Mol Physiol.* 2008;294:L110-120.

89. Franzdottir SR, Axelsson IT, Arason AJ, et al. Airway branching morphogenesis in three dimensional culture. *Respir Res.* 2010;11:162.

90. Dye BR, Dedhia PH, Miller AJ, et al. A bioengineered niche promotes in vivo engraftment and maturation of pluripotent stem cell derived human lung organoids. *Elife.* 2016;5.

91. Chen Y, Feng J, Zhao S, et al. Long-Term Engraftment Promotes Differentiation of Alveolar Epithelial Cells from Human Embryonic Stem Cell Derived Lung Organoids. *Stem Cells Dev.* 2018;27:1339-1349.

92. Acosta JM, Thebaud B, Castillo C, et al. Novel mechanisms in murine nitrofen-induced pulmonary hypoplasia: FGF-10 rescue in culture. *Am J Physiol Lung Cell Mol Physiol.* 2001;281:L250-257.

93. Tan Q, Choi KM, Sicard D, et al. Human airway organoid engineering as a step toward lung regeneration and disease modeling. *Biomaterials.* 2017;113:118-132.

94. Jesudason EC, Connell MG, Fernig DG, et al. In vitro effects of growth factors on lung hypoplasia in a model of congenital diaphragmatic hernia. *J Pediatr Surg.* 2000;35:914-922.

95. Marconett CN, Zhou B, Sunohara M, et al. Cross-Species Transcriptome Profiling Identifies New Alveolar Epithelial Type I Cell-Specific Genes. *Am J Respir Cell Mol Biol.* 2017;56:310-321.

Figure Legends

Figure 1: Human congenital diaphragmatic hernia (CDH) induced pluripotent stem cells (iPSCs) adopted characteristics of 3D lung-like cells, termed lung organoids (LOs). **(A)** Step-wise schematic protocol for the generation of CDH foregut spheroids and LOs (n=10 separate experiments) from iPSCs.[31] All cells were analyzed at serial time points during organoid differentiation using phenotypic markers (shown in the blue boxes). Selected CDH LOs were also exposed to *ex vivo* mechanical compression (red box) at day 35 of differentiation to simulate the compression that occurs *in vivo* from herniated abdominal contents. **(B)** Representative gross appearance of early CDH organoids (*left*) in a 24-well plate (day 4 induction), each measuring 200-500 μm in diameter. Under higher magnification (*right*), phase contrast photomicrographs reveal the typical morphology of organoids derived from CDH iPSCs, magnification, 5x. Scale bar represents 50 μm. **(C)** Representative histology of CDH LOs at day 20 (*left*, magnification, 60x) and day 60 (*right*, magnification, 10x) demonstrates the sac-like architecture that resembles pulmonary alveolar-like tissue [hematoxylin and eosin (H&E) staining]. Scale bar represents 50 μm. **(D)** Vertical bar graph with dot plots of day-28 organoid counts from typical 24-well plates in normal and CDH LOs, ** denotes $p \leq 0.01$ (Mann-Whitney). **(E)** Representative vertical bar graphs with dot plots of serial quantitative gene expression show significant downregulation of the pluripotency-specific genes, *NANOG* and *OCT4*, in representative normal and CDH iPSCs clones

(passage 22-26) after foregut spheroid generation (LO-d0) and during early 3D LO differentiation (LO-d20 and LO-d40). Data were normalized relative to housekeeping gene (*GAPDH*) and presented as the mean±SEM, ** denotes p≤0.01 compared to parental iPSCs (*left bars,* ANOVA), three independent biological replicates (3 separate experiments using 3 different cell lines). Experiments performed without mechanical compression.

Figure 2: In the absence of mechanical compression, human lung organoids (LO) derived from induced pluripotent stem cells (iPSCs) of congenital diaphragmatic hernia (CDH) children revealed baseline impairments in lung differentiation compared to iPSCs of children with normal lungs. **(A)** Representative histology of LOs at day 40 (magnification, 20x) in normal (*left*) and CDH (*right*) iPSCs by [hematoxylin and eosin (H&E) staining]. Scale bar represents 50 μm. **(B)** Vertical bar graph with dot plots of the lung/anterior foregut progenitor gene, *NKX2.1,* shows significant progressive gene upregulation at day 20 and day 40. By day 40, there is a significant increase in LOs derived from children with normal lungs. * and ** denote p≤0.05 and p≤0.01 compared to normal control LOs (ANOVA), n=4-6 per group. **(C)** Representative confocal microscopy sections (magnification, 10x) of human LOs (day 40) derived from normal and CDH iPSCs reveal $NKX2.1^{+}$ cells (TxRed secondary, red or FITC secondary, green) both within and adjacent to clusters of E-cadherin (Ecad)-positive staining. 'L' indicates

luminal structure. Scale bars represent 150 μm. **(D)** Vertical bar graph with dot plots of NKX2.1 protein expression, expressed as a percentage of $DAPI^+$ cells, shows significant downregulation in CDH LOs compared to normal LOs (69.5±5.8% vs. 46.6±4.0%, respectively). * denotes p≤0.05 (Mann-Whitney). **(E)** Vertical bar graph with dot plots of the anterior foregut progenitor gene, *PAX8,* shows minimal gene expression at day 20 and day 40, consistent with specific differentiation towards the pulmonary cell lineage. ** denotes p≤0.01 (ANOVA), n=4-6 per group. **(F)** Representative confocal microscopy section (magnification, 40x) of human LOs (day 40) showing negligible $PAX8^+$ expression (FITC, green). Scale bar represents 50 μm. **(G)** Representative confocal microscopy section (magnification, 10x) indicate both epithelial and mesenchymal components within human LOs (day 40) as suggested by Ecad (Cy5 secondary, white) and αSMA (FITC, green) expression, respectively. Scale bar represents 200 μm. **(H)** Representative confocal microscopy section (magnification, 60x) of CDH LOs (day 40) reveal both $NKX2.1^+$ and type II alveolar epithelial marker, surfactant protein-C^+ (SFTPC) expression (FITC, green). Scale bar represents 10 μm. **(I)** Vertical bar graph with dot plots of SFTPC protein expression shows significant downregulation in CDH LOs compared to normal LOs on day 20. ** denotes p≤0.01 (Mann-Whitney). **(J)** Representative confocal microscopy sections (magnification, 20x) of CDH LOs (day 40, *top*) exhibit peripheral enhancement of cells with type I alveolar epithelial cell marker, podoplanin (PDPN, TxRed, red) in similar pattern to human native

lung tissue (*bottom*). Scale bars represent 25 μm. **(K)** Vertical bar graphs with dot plots show expression of the endodermal gene, *FOXA2* (upper *left*), the mesenchymal gene, vimentin (*VIM*, *upper right*), and key lung epithelial genes, *AQP5* and *SFTPC* (*lower panels*).[95] LO induction was associated with significant upregulation in both mesenchymal and lung epithelial genes. Significant impairment in SFTPC expression was noted amongst CDH LOs. Data were normalized relative to housekeeping gene (*GAPDH*) and presented as the mean±SEM, * and ** denote p≤0.05 and p≤0.01 (ANOVA or Mann-Whitney, as appropriate). Representative from 3 separate experiments using 3 different cell lines. Experiments performed without mechanical compression, and normal human fetal lungs provided as positive controls.

Figure 3: In the absence of mechanical compression, human lung organoids (LO) derived from induced pluripotent stem cells (iPSCs) of congenital diaphragmatic hernia (CDH) children showed differences in lung epithelial and mesenchymal differentiation. **(A)** Representative confocal microscopy sections (magnification, 40x) of CDH LOs (day 40, *left*) indicate positive peripheral cell staining with surfactant protein-C (SFTPC; TxRed secondary, red) in similar pattern to that of human native CDH lung tissue (*middle*). Further evidence of SFTPC lung epithelia is suggested by co-localization with distal epithelial marker, SOX9 (FITC secondary, green; *right*). Scale bars represent 50 μm. **(B)** Vertical bar graph with dot plots of SFTPC protein expression on day 40 reveals

significant downregulation in CDH LOs compared to normal LOs. ** denotes p≤0.01 (Mann-Whitney). **(C)** Representative confocal microscopy sections (magnification, 40x) of CDH LOs (day 60, *top*) suggest positive peripheral cell staining with basal epithelial marker, p63 (FITC secondary, green) and PDPN (TxRed, red) in similar pattern to that of CDH LOs (*bottom*). Scale bars represent 25 μm. **(D,E)** Vertical bar graphs with dot plots on day 40 reveal comparable levels of PDPN and p63 protein expression, respectively, in CDH LOs compared to levels in normal LOs. **(F)** Microarray analysis produced a representative heatmap image documenting alterations in 54 lung development-associated genes (Table S2), grouped based on hierarchical clustering, in day-40 LOs derived from an iPSC clone in a child with normal lungs (LO) compared with day-40 LOs derived from an iPSC clone in a child with CDH (CDH LO). Higher and lower levels of transcripts are shown in red and blue, respectively. three independent biological replicates (3 separate experiments using 3 different cell lines) without mechanical compression. **(G)** Representative heatmap image shows changes in 99 extracellular matrix genes (Table S3), grouped based on hierarchical clustering, in day-40 LOs compared with day-40 CDH LOs. Higher and lower levels of transcripts are shown in red and blue, respectively. Three independent biological replicates (3 separate experiments using 3 different cell lines) without mechanical compression, performed at both day 40 and day 60 timepoints. **(H)** Volcano plot of differentially expressed 54 lung development-associated genes in day-40 LOs derived from an iPSC clone in a child

with CDH. Values are expressed as fold changes in CDH LOs compared with LOs derived from an iPSC clone in a child with normal lungs (shaded area denotes >2-fold change, p-value≤0.05). **(I)** Volcano plot of differentially expressed 99 extracellular matrix-associated genes in day-40 LOs derived from an iPSC clone in a child with CDH. Values are expressed as fold changes in CDH LOs compared with LOs derived from an iPSC clone in a child with normal lungs (shaded area denotes >2-fold change, p-value≤0.05). GEO link: https://www.ncbi.nlm.nih.gov/geo/query/acc.cgi?acc=GSE149780.

Figure 4: In the absence of mechanical compression, human lung organoids (LO) derived from induced pluripotent stem cells (iPSCs) of congenital diaphragmatic hernia (CDH) children showed differences in lung progenitor, proximal, and distal cell differentiation. **(A)** Vertical bar graphs with dot plots of quantitative *SOX2* gene expression show continued upregulation in normal and CDH iPSCs clones for up to 60 days after LO induction (*upper panel*). There was also significant downregulation of the distal lung progenitor marker, *SOX9* (*middle*), and *NKX2.1* (*lower*) in CDH LOs compared to parental iPSC controls. Data were normalized relative to housekeeping gene (*GAPDH*) and presented as the mean±SEM, ** denotes p≤0.01 compared to parental iPSCs (Mann-Whitney), three independent biological replicates (3 separate experiments using 3 different cell lines) without mechanical compression, and normal

human fetal lungs were a positive control. **(B)** Representative confocal microscopy sections (magnification, 40x) of human CDH LOs (day 40, upper *left*) exhibit lung progenitor cell immunostaining patterns with some similarity to human CDH lung (*upper right*), including NKX2.1$^+$ lung progenitors (FITC secondary, green) and endodermal SOX17$^+$ cells (TxRed secondary, red). Scale bars represent 10 μm. A robust E-cadherin$^+$ (Ecad) staining pattern (Cy5 secondary, white) was apparent in CDH LOs at day 40 (*middle left*, magnification, 40x) and day 60 (*lower left*; FITC secondary green; magnification, 20x) analogous to Ecad staining within tissue from infant CDH lungs (*upper right*; Cy5 secondary, white; magnification, 40x), tissue from normal infant lungs (*middle right*; FITC secondary, green; magnification, 40x), and day-60 LOs derived from children with normal lungs (*lower right*, magnification, 60x). Scale bars represent 25 μm. 'L' indicates the lumen. **(C)** Representative vertical bar graph of quantitative *Ki67* gene expression shows continued expression of this cellular proliferation marker in both normal and CDH iPSCs clones for up to 60 days after LO induction (*upper panel*). Data were normalized relative to housekeeping gene (*GAPDH*), presented as the mean±SEM, * denotes p≤0.01 compared to parental iPSC controls (Student's t-test), and three independent biological replicates without mechanical compression (3 separate experiments using 3 different cell lines). **(D)** Representative confocal sections at day 40 show microscopic CDH LO lumen lined with SFTPC$^+$ cells (FITC secondary, green) and Ki67$^+$ cells (TxRed secondary, red) along its periphery and evidence of a

vimentin (VIM)$^+$ stroma (Cy5 secondary, white; *top*, magnification, 20x). High power image of CDH LO reveal robust Ki67$^+$ cells (TxRed secondary, red) and endodermal SOX17$^+$ cells (Cy5 secondary, white) with scant activated caspase 3 (Cas3)$^+$ cells (FITC secondary, green; *bottom*, magnification, 60x). Scale bars represent 10 μm. 'L' indicates the lumen.

Figure 5: In the absence of mechanical compression, human lung organoids (LO) derived from induced pluripotent stem cells (iPSCs) of congenital diaphragmatic hernia (CDH) children showed differences in lung epithelial and mesenchymal cell differentiation. **(A)** Vertical bar graphs of serial quantitative RT-PCR confirmed the expression of distal lung epithelial-associated genes in normal and CDH LOs, demonstrating upregulation compared to parental iPSCs but significantly decreased expression of type II alveolar epithelial cells, including surfactant protein-B (*SFTPB, left*) and surfactant protein-C (*SFTPC, middle*), in CDH LOs at both 40 and 60 days after LO induction. Expression of the type I alveolar epithelial cell marker, podoplanin (*PDPN, right*), was similar between LOs and CDH LOs in multiple timepoints. Data were normalized relative to housekeeping gene (*GAPDH*) and presented as the mean±SEM, ** denotes p≤0.01 (ANOVA and Mann-Whitney, as appropriate), n=4 independent biological replicates (3 separate experiments using 3 different cell lines) without mechanical compression, and human fetal normal lung as a positive control. **(B)**

Representative confocal microscopy sections of human amniotic fluid-derived CDH LOs (day 40) reveal multiple proximal and distal lung progenitor cell types within a surrounding mesenchyme. There are $SOX9^+SFTPC^+$ cells (FITC/TxRed secondary, green/red) lining a sac-like structure within αSMA^+ mesenchyme (*top row, left*; Cy5, white; magnification, 40x). 'L' indicates luminal structure. Acetylated alpha-tubulin (αTUB; Txred secondary, red) positive staining of ciliary epithelium adjacent to $NKX2.1^+$ cells (FITC, green; *top row, right*; magnification, 20x). High-power image demonstrates proximal airway-like stratified epithelium E-cadherin $(Ecad)^+$ (TxRed, red) with continued expression of $NKX2.1^+$ progenitors and $SOX17^+$ cells (*second row, left*; FITC/Cy5, green/white); magnification, 60x). There are $p63^+$ (bronchial reserve) cells (FITC, green) completely lining the outside of sac-like structures within a background of plate-like $PDPN^+$ and more rounded $MUC5b^+$ goblet cells (*second row, right*; TxRed/Cy5, red/white; magnification, 20x). Robust staining of α-smooth muscle actin (αSMA) and secretory PLUNC (TxRed/Cy5, red/white) near $p63^+$ cells (FITC, green), suggestive of proximal lung epithelium (*third row, left*; magnification, 60x). The presence of multiple proximal airway cell types, as shown by club cell secretory protein (CCSP) and FOXJ1 (TxRed/Cy5, red/white), is shown (*third row, right*; magnification, 40x). Scale bars represent 10 μm. 'L' indicates the lumen. **(C)** High-power confocal images revealing well-organized $PDGFR\alpha^+/VIM^+$ cells (FITC/Cy5, green/white), indicative of myofibroblastic differentiation, along the periphery of a $PLUNC^+$ luminal structure

(TxRed, red; magnification, 60x). **(D)** Vertical bar graphs with dot plots of serial quantitative mesenchymal gene expression in amniotic fluid-derived normal and CDH LOs show upregulation of *VIM*, α*SMA*, and *PDGFR*α compared to parental iPSCs. Whereas expression of *VIM* (*top)* and α*SMA* (*middle*) were similar between LOs and CDH LOs, there was significantly decreased expression of *PDGFR*α *(bottom*) in CDH LOs at both day 40 and day 60. Data were normalized relative to housekeeping gene (*GAPDH*) and presented as the mean±SEM, ** denotes p≤0.01 compared to normal LOs at same induction time (Mann-Whitney), two independent biological replicates without mechanical compression (3 separate experiments using 3 different cell lines).

Figure 6: *Ex vivo* mechanical compression was associated with alterations in human congenital diaphragmatic hernia lung organoid (CDH LO) epithelial and mesenchymal gene regulation. **(A)** Schematic representation of the compression device, in which day-40 CDH LOs (*left*) are exposed to static compression [*middle*, adapted from [33]] to simulate *in utero* forces (*right*). Scale bar represents 100 μm. **(B)** Representative low-power photomicrographs of CDH LOs under static mechanical compression (400 Pa) for 48 hrs (*bottom row*). Controls consisting of CDH LOs derived from the same iPSC clones but without mechanical compression were cultured in parallel (*top row*). CDH LOs reveal no obvious differences with respect to hematoxylin and eosin (H&E, *left panels*) after mechanical compression. Active Ki67/caspase-3 (Cas3)

immunofluorescent staining (*middle panels*; TxRed/FITC secondary, red/green) confirms ongoing cell proliferation and apoptosis in both groups. Confocal images illustrate SOX9 (Cy5 secondary, white) and α-smooth muscle actin (αSMA; TxRed secondary, red) distributed throughout the entire LO, regardless of mechanical compression (*right panels*). Scale bars represent 50 μm. **(C)** Vertical bar graphs with dot plots show quantitative gene expression in normal LOs (black bars) and CDH LOs (white bars) under two different static mechanical compression forces (+ = 200 Pa vs. ++ = 400 Pa) for 48 hrs. Mechanical compression at 400 Pa was associated with significant downregulation of podoplanin (*PDPN*) but not surfactant protein-C (*SFTPC*) when compared to non-compression controls (- = 0 Pa). Data were normalized relative to housekeeping gene (*GAPDH*) and presented as the mean±SEM. ** denotes p≤0.01 compared to the respective non-compressed LOs (Mann Whitney), independent biological replicates (n=3 for CDH LOs, n=2 for normal LOs). **(D)** Higher mechanical compression was associated with significant downregulation in *Ki67* and *NKX2.1* but differential responses in *FOXA2*. ** denotes p≤0.01 compared to the respective non-compressed LOs (ANOVA). **(E)** Higher mechanical compression was associated with significant upregulation in vimentin (*VIM*) that was specific to CDH LOs but differential responses in PDGFRα. * and ** denote p≤0.05 and p≤0.01, respectively (ANOVA).

Figure 7: Further evidence that ex *vivo* mechanical compression altered human congenital diaphragmatic hernia lung organoid (CDH LO) epithelial and mesenchymal development. **(A)** Vertical bar graphs with dot plots show significant downregulation of *SOX2* and *SOX9* gene expression in CDH and normal LOs under two different static mechanical compression forces (+ = 200 Pa vs. ++ = 400 Pa) for 48 hrs. Mechanical compression downregulates both *SOX2* and *SOX9* expression in a pressure-dependent manner. Data were normalized relative to housekeeping gene (*GAPDH*) and presented as the mean±SEM, * and ** denote $p \leq 0.05$ and $p \leq 0.01$, respectively, independent biological replicates (n=3 for CDH LOs, n=2 for normal LOs). **(B)** Representative confocal microscopy sections (magnification, 10x) of LOs and CDH LOs after exposure to 200 Pa of mechanical compression, showing E-cadherin (Ecad) and NKX2.1 protein expression (FITC and TxRed secondary, green/red). Scale bars represent 150 μm. **(C)** Vertical bar graph with dot plots of NKX2.1 protein expression before and after mechanical compression reveals differential responses between LOs and CDH LOs. * denotes $p \leq 0.05$ (Mann-Whitney). **(D)** Vertical bar graphs with dot plots of selected protein expression before and after mechanical compression show significant downregulation in SOX9. ** denotes $p \leq 0.01$ (Mann-Whitney). **(E)** Representative confocal microscopy sections (magnification, 60x) after exposure to 400 Pa of mechanical compression, demonstrating E-cadherin (Ecad) and robust vimentin (VIM)

staining (Cy5 and FITC secondary, white/green) in CDH LOs. Scale bars represent 25 μm.

Supporting Information

Additional supporting information may be found online in the Supporting Information section at the end of the article.

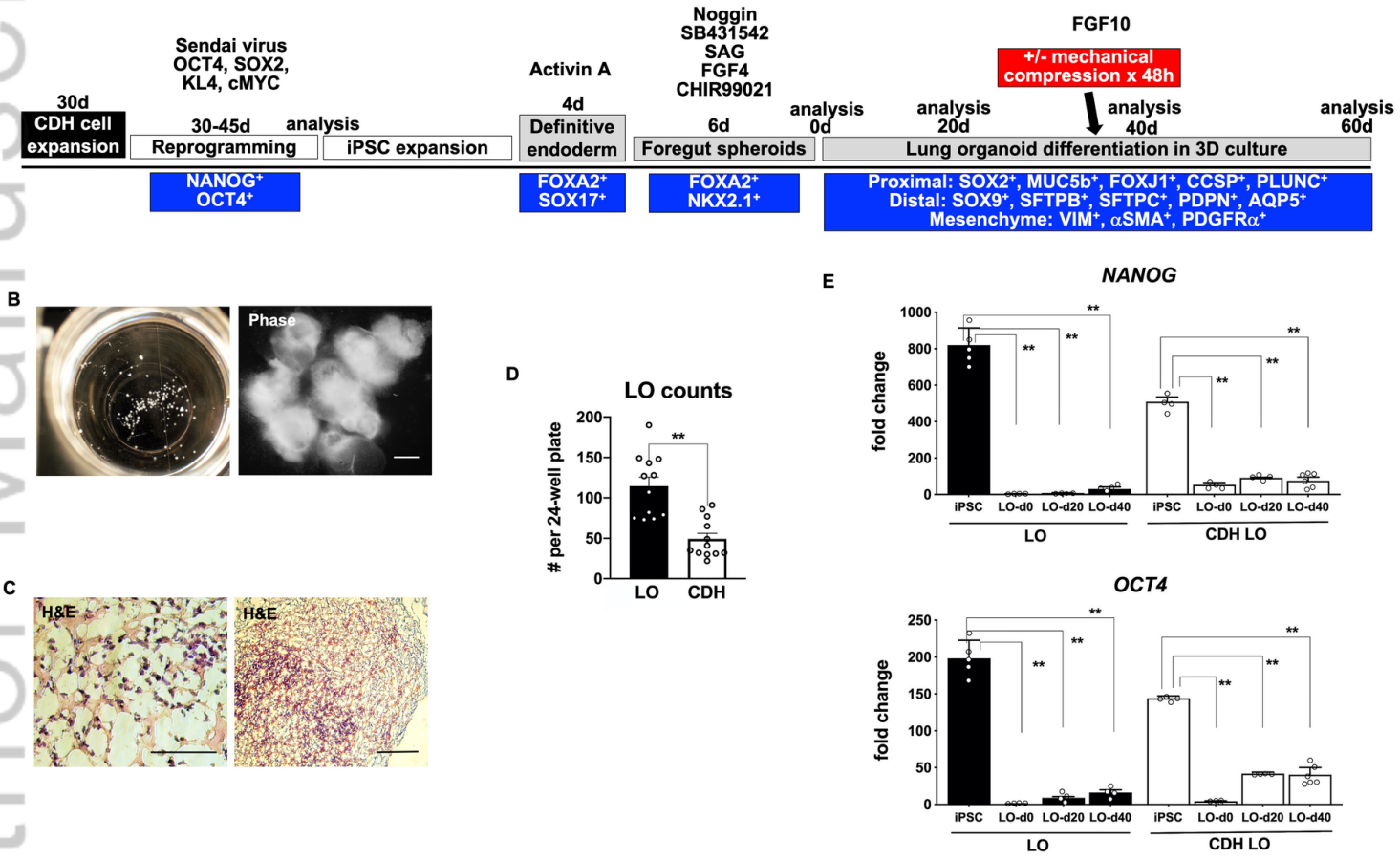

SCT3_12826_FIGURE_1.tif

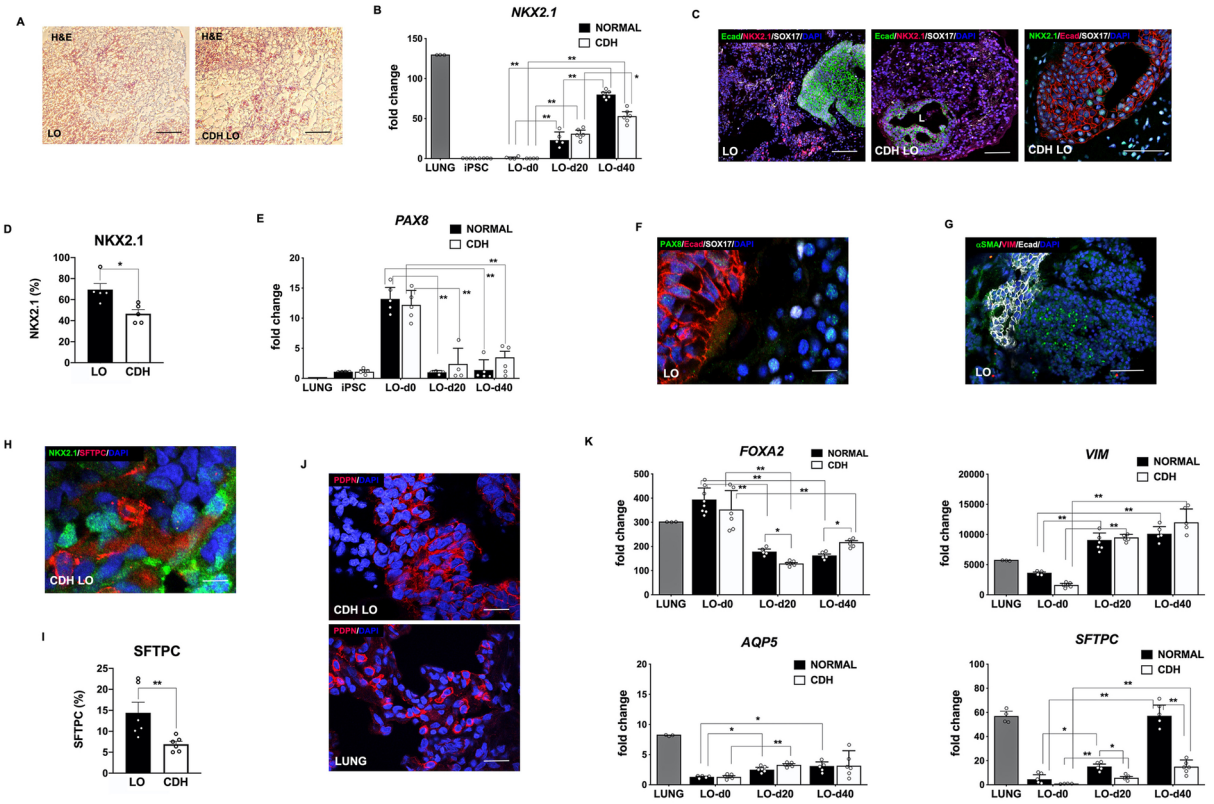

SCT3_12826_FIGURE_2.tif

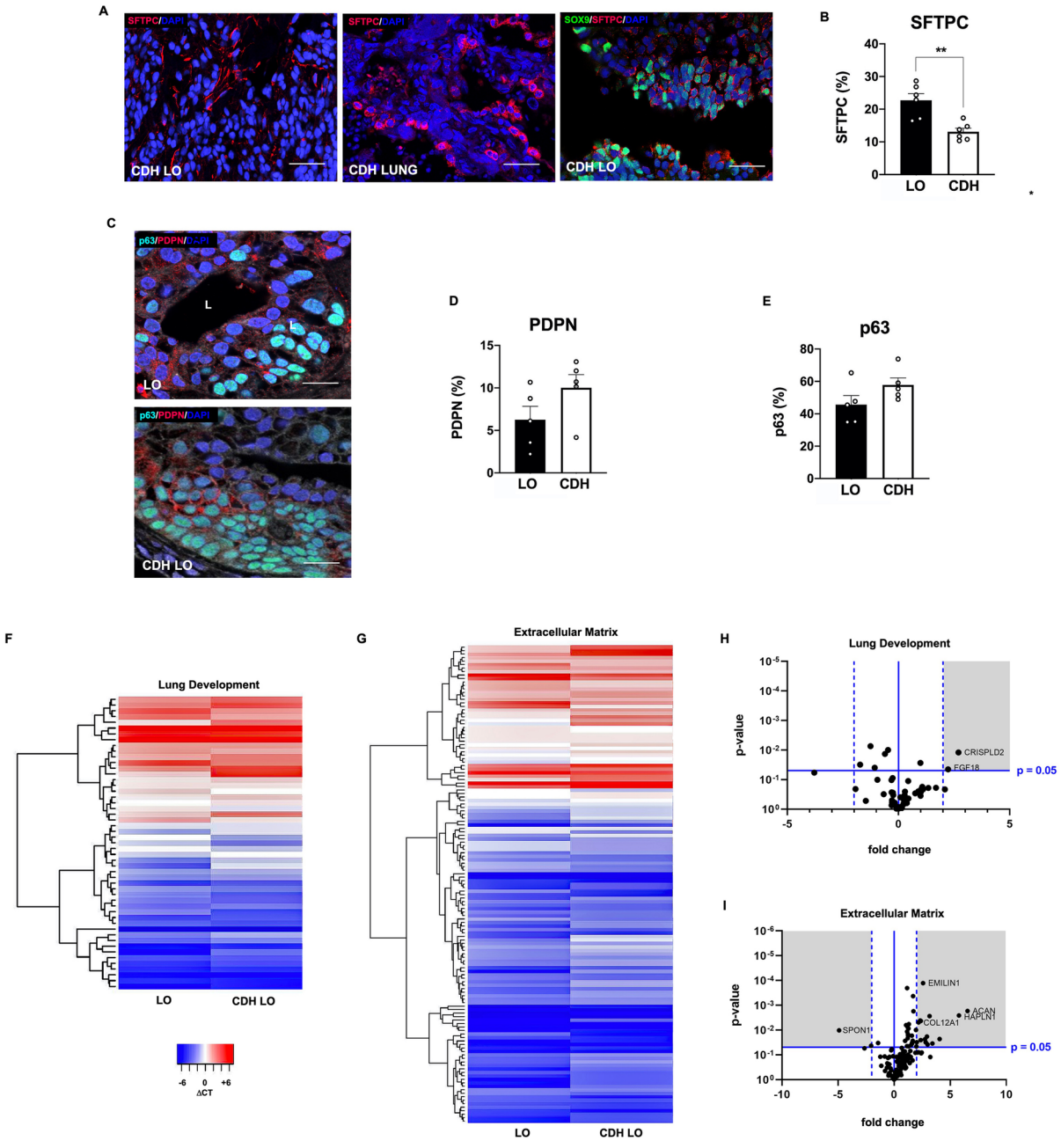

SCT3_12826_FIGURE_3.tif

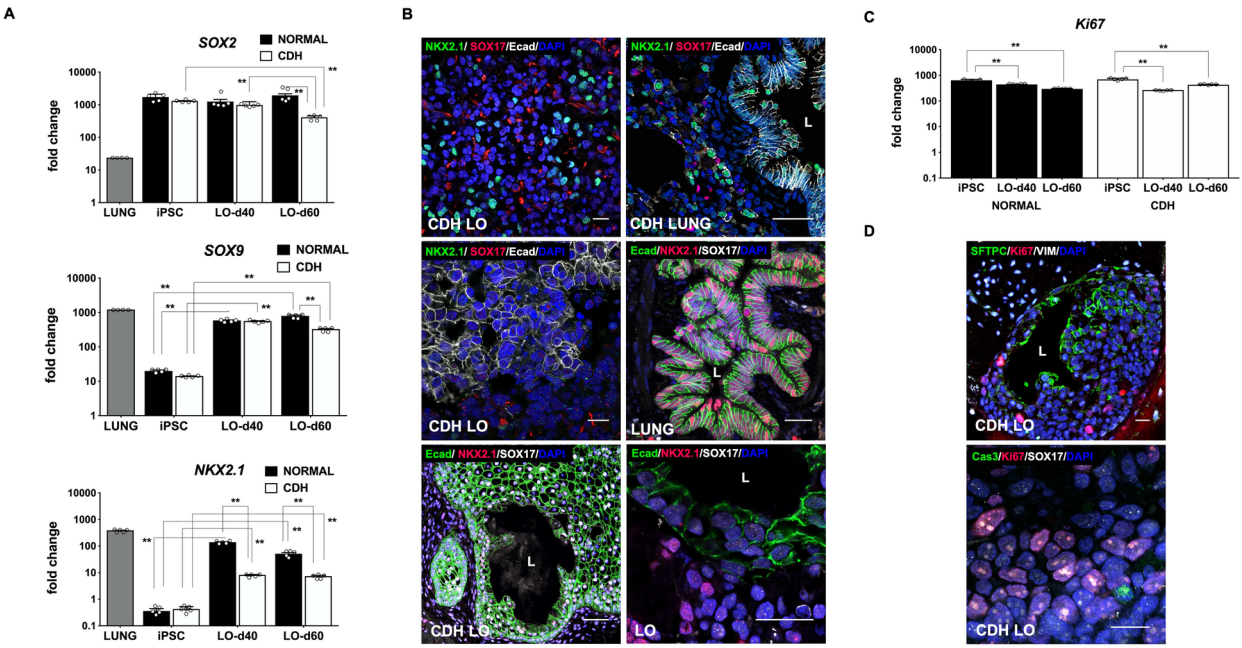

SCT3_12826_FIGURE_4.tif

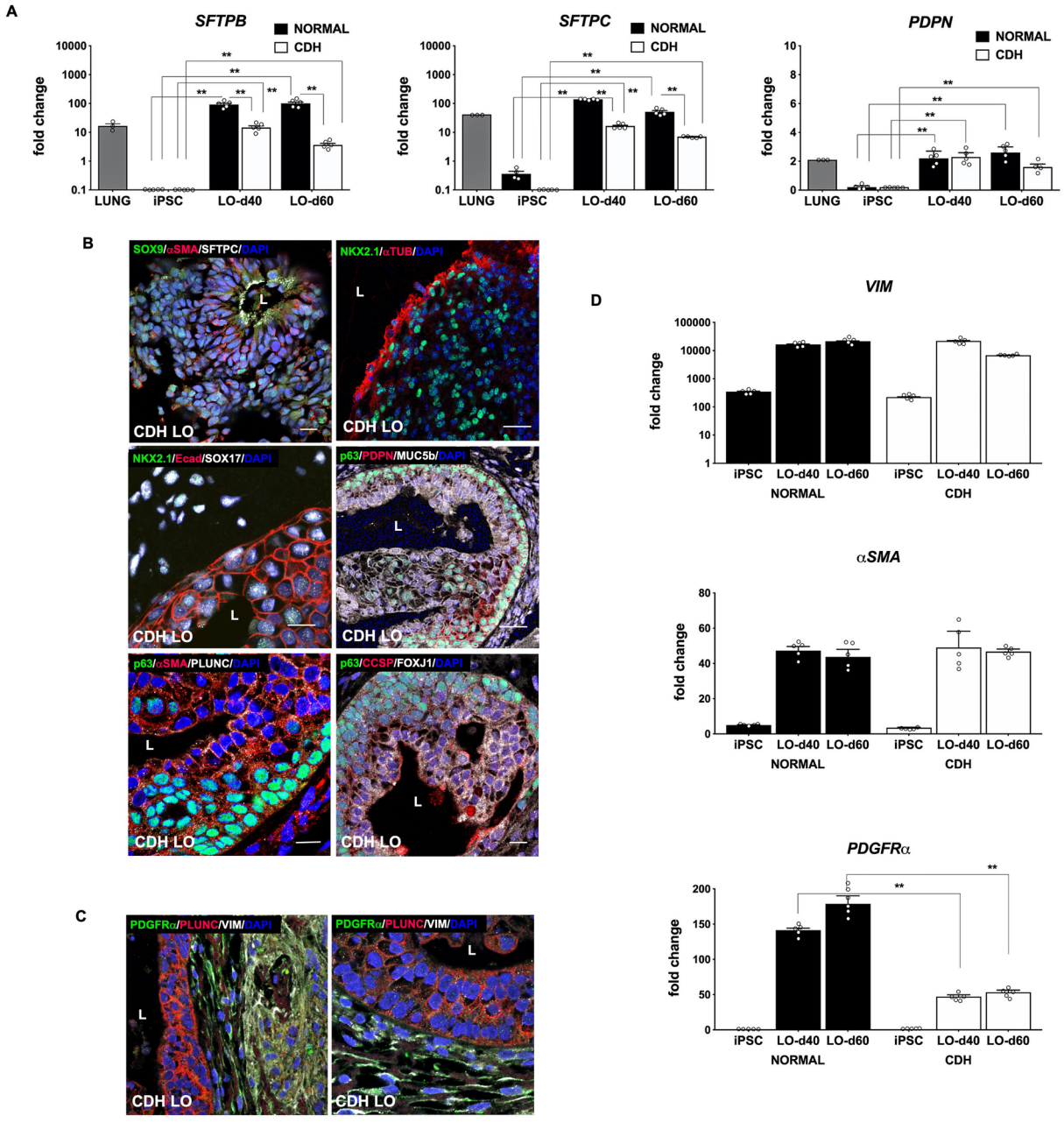

SCT3_12826_FIGURE_5.tif

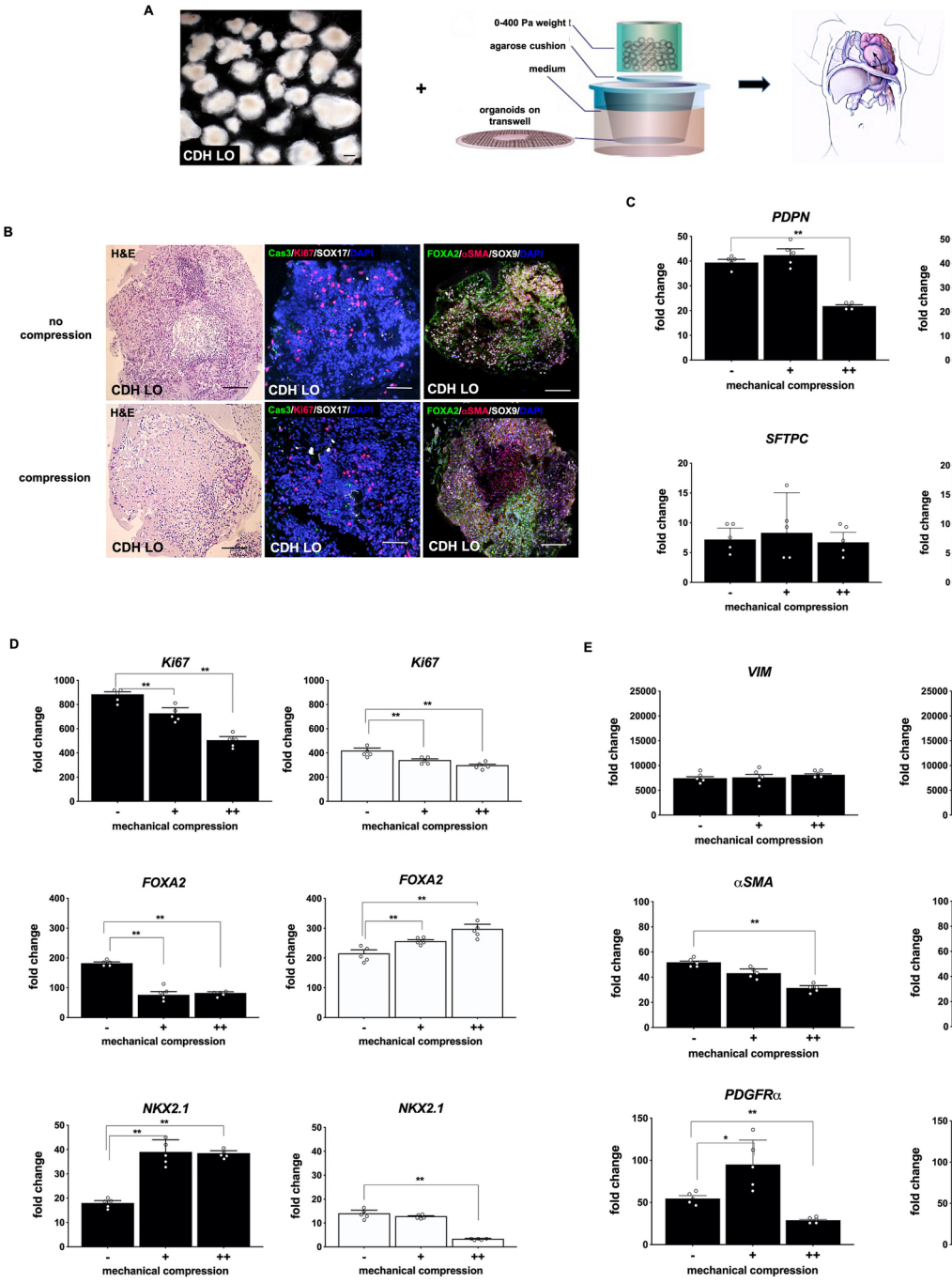

SCT3_12826_FIGURE_6.tif

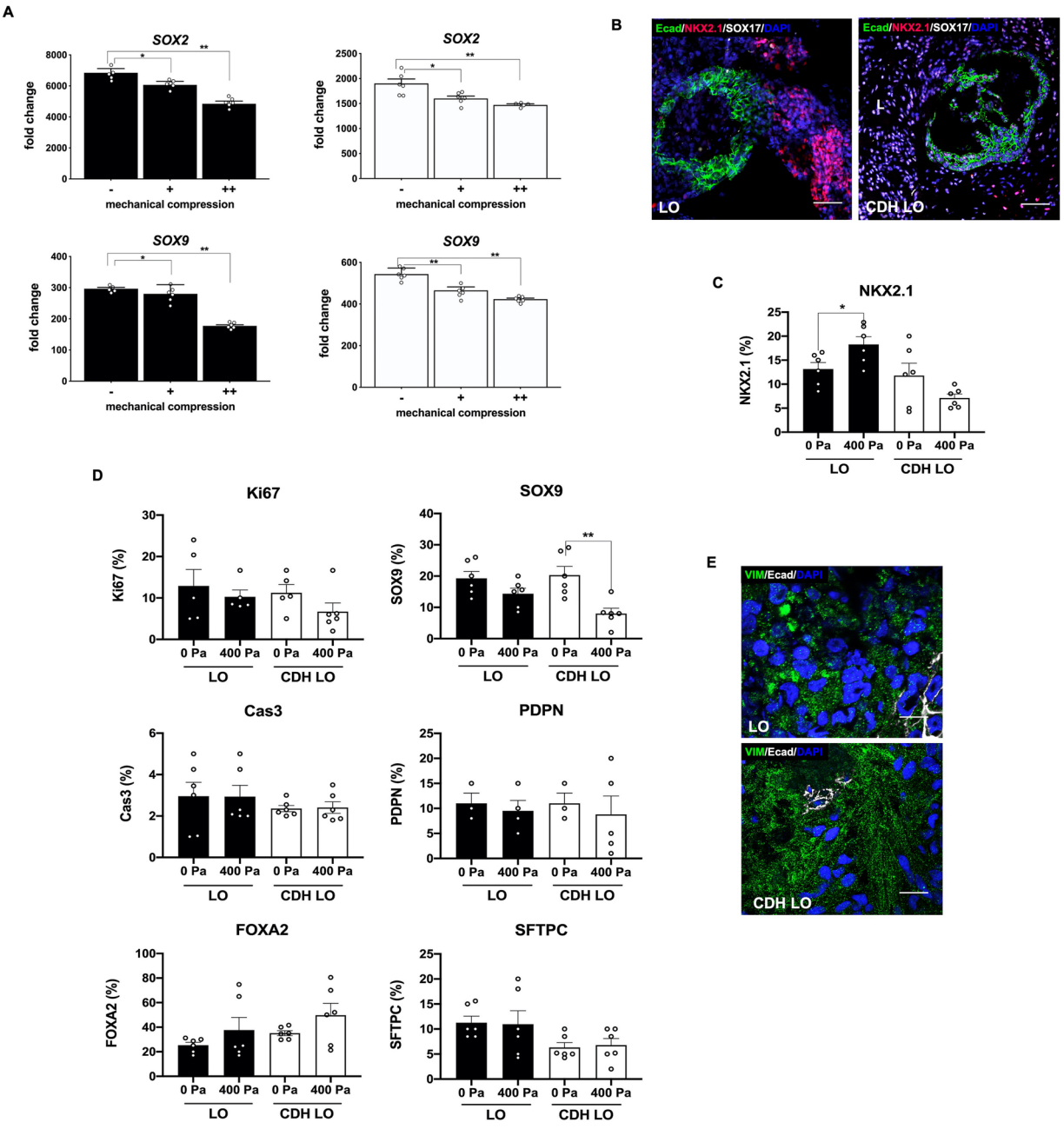

SCT3_12826_FIGURE_7.tif

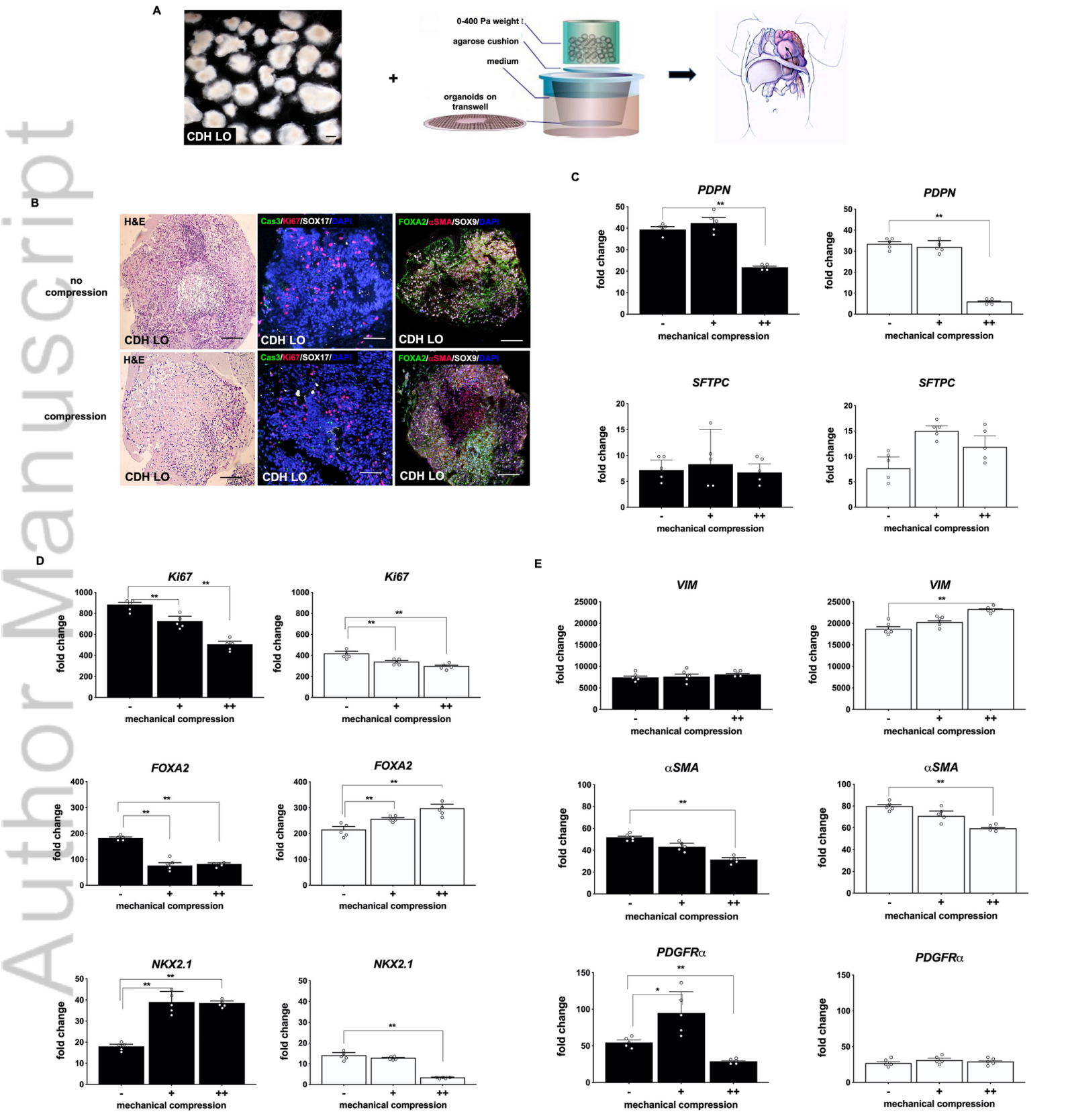

SCT3_12826_Graphical abstract KUNISAKI.tif